

## RESEARCH OUTPUTS / RÉSULTATS DE RECHERCHE

### First hyperpolarizability of the di-8-ANEPPS and DR1 nonlinear optical chromophores in solution

Bouquiaux, Charlotte; Beaujean, Pierre; Ramos, Tarcus N.; Castet, Frederic; Rodriguez, Vincent; Champagne, Benoît

*Published in:*

The Journal of chemical physics

*DOI:*

[10.1063/5.0174979](https://doi.org/10.1063/5.0174979)

*Publication date:*

2023

*Document Version*

Peer reviewed version

[Link to publication](#)

*Citation for published version (HARVARD):*

Bouquiaux, C, Beaujean, P, Ramos, TN, Castet, F, Rodriguez, V & Champagne, B 2023, 'First hyperpolarizability of the di-8-ANEPPS and DR1 nonlinear optical chromophores in solution: An experimental and multi-scale theoretical chemistry study', *The Journal of chemical physics*, vol. 159, no. 17, 174307. <https://doi.org/10.1063/5.0174979>

#### General rights

Copyright and moral rights for the publications made accessible in the public portal are retained by the authors and/or other copyright owners and it is a condition of accessing publications that users recognise and abide by the legal requirements associated with these rights.

- Users may download and print one copy of any publication from the public portal for the purpose of private study or research.
- You may not further distribute the material or use it for any profit-making activity or commercial gain
- You may freely distribute the URL identifying the publication in the public portal ?

#### Take down policy

If you believe that this document breaches copyright please contact us providing details, and we will remove access to the work immediately and investigate your claim.

**Investigation of the First Hyperpolarizability of the di-8-ANEPPS Nonlinear Optical Probe in Solution. An Experimental and Multi-Scale Theoretical Chemistry Study**

Charlotte Bouquiaux,<sup>1</sup> Tárcius Nascimento Ramos,<sup>1</sup> Frédéric Castet,<sup>2</sup> Vincent Rodriguez,<sup>2, a)</sup> and Benoît Champagne<sup>1, b)</sup>

*<sup>1)</sup>University of Namur, Theoretical Chemistry Lab, Unit of Theoretical and Structural Physical Chemistry, Namur Institute of Structured Matter, rue de Bruxelles, 61, B-5000 Namur (Belgium)*

*<sup>2)</sup>University of Bordeaux, Institut des Sciences Moléculaires, UMR 5255 CNRS, cours de la Libération 351, F-33405 Talence Cedex (France)*

(Dated: August 9, 2023)

The effects of solvent polarity on the linear and nonlinear optical properties of an aminonaphthylethynylpyridinium (ANEP) dye have been investigated by combining experimental and theoretical chemistry methods. Indeed, measurements are usually not performed in gas phase but in condensed phases such as solutions, so that it is of great importance both to monitor these effects and to assess how solvent models can account for these. On the one hand, Deep-Near Infrared (NIR) Hyper-Rayleigh scattering (HRS) measurements (1840-1950 nm) were performed on solutions of di-8-ANEPPS in  $\text{DCCl}_3$ , DMF, and DMSO. In particular, for the first time, HRS experiments have been performed in the picosecond regime in the Deep-NIR with very moderate ( $\leq 3$  mW) average input power. These are compared with theoretical results obtained by using a sequential molecular dynamics (MD) then quantum mechanics (QM) approach. The MD method allows accounting for the dynamical nature of the molecular structures. Then, the QM part is based on TDDFT/M06-2X/6-311+G\* calculations using several solvation models ranging from continuum to discrete ones. Both measurements and calculations extend our knowledge of the NLO responses of di-8-ANEPPS in the long wavelengths regime, information that is currently lacking. Similarly, the effects of frequency dispersion on the NLO properties of a commonly used HRS reference dye, DR1, are investigated. For di-8-ANEPPS and DR1, comparisons show that the use of an "intermediate" scheme, combining the description of the solvent molecules around the probe by point charges with a continuum model, already achieves quasi quantitative agreement with the experimental data, and is therefore an efficient choice. Moreover, if computational resources allow, the results can be further improved by using a polarizable embedding that includes the atomic polarizabilities in the solvent description. With this work, we provide new sets of experimental and calculated NLO responses of push-pull probes to assess how best to account for solvent and frequency dispersion effects.

---

<sup>a)</sup>vincent.rodriquez@u-bordeaux.fr

<sup>b)</sup>benoit.champagne@unamur.be

## I. INTRODUCTION

Donor- $\pi$ -acceptor molecules are the prototype of second-order nonlinear optical (NLO) compounds that can exhibit large second harmonic generation (SHG) responses. Owing to their interest in optical data processing,<sup>1</sup> in laser sources, as well as in bioimaging,<sup>2-7</sup> the understanding, control, and optimization of the underlying NLO responses is of primary importance. So, many studies, either experimental or combining quantum chemistry characterizations have helped deducing structure-property relationships (*e.g.* donor and acceptor strengths, nature of the  $\pi$ -conjugated segment).<sup>3,8-17</sup> Since the experimental determination of their properties is generally not performed in gas phase but in condensed phases, it is also necessary to assess how the environment influences the NLO responses. Focusing the most common environments (*i.e.* solutions), experimental studies have shown that solvent effects can considerably affect the response of the NLO emitters. This was demonstrated for parnitroaniline (PNA), a common NLO reference,<sup>18-21</sup> retinal,<sup>22</sup> donor-acceptor polyenes,<sup>23</sup> thiophene chromophores,<sup>24</sup> organic acids,<sup>25</sup> etc. From these studies, larger NLO responses have been associated with more polar solvents, *e.g.* the NLO response of retinal is enhanced by more than a factor 10 when going from dioxane to nitromethane.<sup>22</sup> In this context, it is important to assess how current theoretical solvation models are able to characterize the NLO responses of organic probes in solution. Many methods have been developed to account for solvent effects in quantum chemical calculations and are available in a number of software packages. They differ in the way the solvent as well as its interactions with the solute are described and range from discrete to continuum approaches.<sup>26</sup> On the one hand, the solvent molecules are explicitly considered, either at a quantum mechanical (QM) or molecular mechanics (MM) - *i.e.* classical mechanics - level. Since it is not possible to include all the molecules that make up the liquid, approximations are required to perform the calculations.<sup>26</sup> This led, for instance, to the development of the Supermolecular (SM)<sup>27</sup> approach. It is also with this in mind that QM/MM approaches have been developed. These multi-scale, also called hybrid, methods were first introduced by Warshel and Levitt in 1976,<sup>28</sup> and awarded them and Karplus the Nobel Prize in Chemistry in 2013.<sup>29</sup> Generally, those models provide a balance between accuracy and efficiency to achieve a realistic description of the system. They also allow considering system sizes that are impossible to treat at the full QM level. QM/MM schemes model the solute "active site" where the target phenomena take place at the QM level, but take advantage of a simpler description for the remaining part. In most QM/MM schemes, the QM region is polarized

by the MM region by using an Electrostatic Embedding (EE),<sup>30</sup> that includes the usually dominant electrostatic contributions but not the induction ones. These missing induction contributions can be included by associating site polarizabilities on the surrounding molecules and computing self-consistently the induced dipole moment between the QM and MM regions. This is known as the Polarizable Embedding (PE) scheme.<sup>31</sup> On the other hand, in implicit schemes, the solvent is modeled by a polarizable continuum medium described by its macroscopic properties, *e.g.* the dielectric constant.<sup>32</sup> In that case, the idea of individual solvent molecules is lost. Among these, popular approaches based on the apparent surface charges (ASC) method include the Polarizable Continuum Model (PCM),<sup>32–35</sup> the Solvation Model Density (SMD),<sup>36</sup> and the Conductor-like Screening Model (COSMO).<sup>37–39</sup> In addition, multiple solvation models can be combined to treat different "layers" of the system using different levels of approximation. This leads to cluster continuum models or micro-solvation schemes.<sup>40,41</sup> These can also be generalized within the Own N-layered Integrated molecular Orbitals and Molecular mechanics (ONIOM) approach.<sup>42</sup>

Focusing on the NLO responses, it has been shown that electrostatic interactions play a key role in modulating the  $\beta$  responses of an embedded molecule.<sup>43–50</sup> Since these are long-range effects, they are nearly impossible to retrieve using QM-only schemes, as a prohibitive number of solvent molecules should be included. Fortunately, good agreement with experiment can generally be obtained using an "intermediate" or "low" solvent description. Indeed, linear and nonlinear responses obtained using continuum or QM/MM models are, in many cases, able to reproduce trends and even quantitative experimental values.<sup>15,49–56</sup> As a result, they have been used to evaluate the NLO properties of a wide variety of systems: pure solvents,<sup>49,50,54</sup> probes embedded in lipid bilayers,<sup>57–61</sup> organic molecules in solutions,<sup>17,45–47,56,62–66</sup> and more recently on liquid air interfaces.<sup>49,67</sup> In fact, PCM is one of the most effective and widely used method for describing the solvent effects on the electronic structure, the geometry, as well as the properties of molecules in solution.<sup>68</sup>

Herein we present a study of the solvent effects on the first hyperpolarizability of two push-pull chromophores: one hemicyanine dye, 4-2-[6-(dibutylamino)-2-naphthalenyl]- ethenyl-1-(3-sulfopropyl)pyridinium inner salt (di-8-ANEPPS), and one azobenzene dye, disperse red 1 (DR1) (Figure 1). These compounds consist of an electron acceptor group connected by a  $\pi$ -conjugated segment to an electron donor group.<sup>23,69</sup> Di-8-ANEPPS is of particular interest because it is often used as a biocompatible probe to investigate membrane morphology<sup>2,3,70–72</sup> and membrane potential.<sup>73–75</sup> Solvent effects on the linear and nonlinear optical properties of hemicyanine-type

Sample title

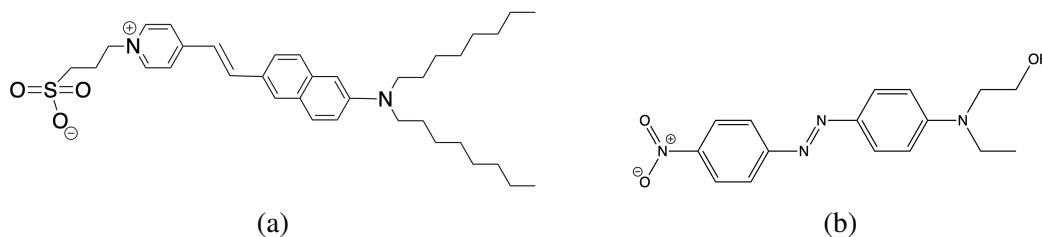


Figure 1: Structures of **(a)** di-8-ANEPPS, and **(b)** DR1.

chromophores have already been investigated, but those studies are often missing the description of the dynamical characteristics of the solvent.<sup>76–80</sup> Besides, they mainly used PCM<sup>76–83</sup> or QM/MM,<sup>81</sup> and mainly focused on the linear optical responses and not on the nonlinear ones. On the other hand, DR1 is a chromophore commonly employed as external reference in NLO measurements<sup>84–95</sup> so that many experimental values are available.<sup>13,20,84,93,96–103</sup> This is however not the case for di-8-ANEPPS, for which only the first hyperpolarizability in DMSO is available.<sup>92</sup> However experimental values have been obtained using high-energy incident light (between 800 nm and 1064 nm), near the two-photon resonance region. Moreover, the characterization of those dyes is also lacking theoretical work focusing on their NLO properties.

In this context, a joint experimental - quantum chemical investigation of the first hyperpolarizabilities,  $\beta$ , of both di-8-ANEPPS and DR1 has been carried out.  $\beta$  of di-8-ANEPPS has been measured in various solvents [deuterated chloroform (DCCl<sub>3</sub>), dimethylsulfoxide (DMSO), and dimethylformamide (DMF)], while  $\beta$  of DR1 was characterized in DCCl<sub>3</sub>. The experimental characterizations have been carried out using Hyper-Rayleigh scattering (HRS) measurements. On the other hand, a sequential MM+QM<sup>104</sup> method was enacted to evaluate  $\beta$ . Several solvation models, namely EE, PE, PCM, and SMD, were used and compared.

## II. EXPERIMENTAL AND THEORETICAL BACKGROUND

### A. Aspects of Nonlinear Optics and HRS Measurements

For isotropic media such as gases and solutions, the most widely used method to measure SHG responses is based on the Hyper-Rayleigh Scattering (HRS) phenomenon, which is an incoherent second-order NLO process. Although coherent SHG is forbidden in isotropic media for symmetry reasons, incoherent HRS is allowed because the non-centrosymmetric molecules act as individual and uncorrelated scattering centers.<sup>18,94,105</sup>

Sample title

The principle of the experiment is that the intensity of the total second harmonic scattered light,  $I^{2\omega}$ , is related to squares of the individual molecular first hyperpolarizability,  $\beta$ , and to the square of the intensity of the incident light,  $I^\omega$ . So, for a binary solution [solvent ( $S$ ) and solute ( $X$ )] in the diluted regime, where both  $S$  and  $X$  generate a  $\beta$  response,  $I^{2\omega}$  is given by:

$$I_{2\omega}^{\Psi V} = G f_L^2 \{C_S |\beta_S|^2 C_{\Psi V}^S + C_X |\beta_X|^2 C_{\Psi V}^X\} (I_\omega T_\omega)^2 10^{-\varepsilon_{2\omega}^X d C_X} \quad (1)$$

where  $G$  is a constant containing geometrical, optical, and electrical factors of the experimental set-up,  $C$  is the concentration of the solvent or solute,  $f_L$  is a local field correction approximated using the high-frequency Lorentz—Lorenz spherical cavity expression, which includes the refractive index of the solvent at the optical frequencies  $\omega$  and  $2\omega$ ,  $T_\omega$  is the transmission loss due to the absorption of the fundamental beam at  $\omega$ ,  $\varepsilon_{2\omega}$  accounts for the one-photon absorption of the chromophore at the second harmonic frequency,  $d$  is the optical path of the scattered harmonic light, and  $\Psi$  characterizes the state of polarization of the incident light.  $\Psi = 0^\circ$  ( $90^\circ$ ) corresponds to a linear horizontal [H] (vertical [V]) polarization.  $C_{\Psi V}$  corresponds to the orientational averages of the spherical components of the molecular first hyperpolarizability tensor of the solvent/solute.

Assuming a linearly polarized incident light propagating along the X direction, characterized by the polarization angle  $\Psi$ , the intensity of the harmonic light scattered at  $90^\circ$  (along the Y direction), and vertically (V) polarized (along the Z axis) is given by the Bershon's expression:<sup>106</sup>

$$I_{\Psi V}^{2\omega} \propto \langle \beta_{ZXX}^2 \rangle \cos^4 \Psi + \langle \beta_{ZZZ}^2 \rangle \sin^4 \Psi + \cos^2 \Psi \sin^2 \Psi \langle (\beta_{ZXZ} + \beta_{ZZX})^2 + 2\beta_{ZZZ}\beta_{ZXX} \rangle \quad (2)$$

where the brackets indicate an averaging over all possible molecular orientations. In this setup, the angle of the plane of polarization of the incident beam,  $\Psi$ , is practically implemented by the rotation of  $\Psi/2$  of a half-wave plate (HWP). The orientational averages involved in Eq. 2 can be simplified and expressed as follows:

$$\langle (\beta_{ZXZ} + \beta_{ZZX})^2 + 2\beta_{ZZZ}\beta_{ZXX} \rangle = \langle \beta_{ZZZ}^2 \rangle + \langle \beta_{ZXX}^2 \rangle \quad (3)$$

and the orientational invariants can be expressed in terms of the molecular components of the  $\beta$  tensor:

$$\begin{aligned}
\langle \beta_{ZZZ}^2 \rangle &= \frac{1}{7} \sum_i^{x,y,z} \beta_{iii}^2 + \frac{4}{35} \sum_{i \neq j}^{x,y,z} \beta_{iij}^2 + \frac{2}{35} \sum_{i \neq j}^{x,y,z} \beta_{iii} \beta_{ijj} + \frac{4}{35} \sum_{i \neq j}^{x,y,z} \beta_{jii} \beta_{iij} \\
&+ \frac{4}{35} \sum_{i \neq j}^{x,y,z} \beta_{iii} \beta_{jji} + \frac{1}{35} \sum_{i \neq j}^{x,y,z} \beta_{jii}^2 + \frac{4}{105} \sum_{i \neq j \neq k}^{x,y,z} \beta_{iij} \beta_{jkk} + \frac{1}{105} \sum_{i \neq j \neq k}^{x,y,z} \beta_{jii} \beta_{jkk} \\
&+ \frac{4}{105} \sum_{i \neq j \neq k}^{x,y,z} \beta_{iij} \beta_{kkj} + \frac{2}{105} \sum_{i \neq j \neq k}^{x,y,z} \beta_{ijk}^2 + \frac{4}{105} \sum_{i \neq j \neq k}^{x,y,z} \beta_{ijk} \beta_{jik}. \\
\langle \beta_{ZXX}^2 \rangle &= \frac{1}{35} \sum_i^{x,y,z} \beta_{iii}^2 + \frac{4}{105} \sum_{i \neq j}^{x,y,z} \beta_{iij} \beta_{ijj} - \frac{2}{35} \sum_{i \neq j}^{x,y,z} \beta_{iii} \beta_{jji} + \frac{8}{105} \sum_{i \neq j}^{x,y,z} \beta_{iij}^2 \\
&+ \frac{3}{35} \sum_{i \neq j}^{x,y,z} \beta_{ijj}^2 - \frac{2}{35} \sum_{i \neq j}^{x,y,z} \beta_{iij} \beta_{jii} + \frac{1}{35} \sum_{i \neq j \neq k}^{x,y,z} \beta_{ijj} \beta_{ikk} - \frac{2}{105} \sum_{i \neq j \neq k}^{x,y,z} \beta_{iik} \beta_{jjk} \\
&- \frac{2}{105} \sum_{i \neq j \neq k}^{x,y,z} \beta_{iij} \beta_{jkk} + \frac{2}{35} \sum_{i \neq j \neq k}^{x,y,z} \beta_{ijk}^2 - \frac{2}{105} \sum_{i \neq j \neq k}^{x,y,z} \beta_{ijk} \beta_{jik} \tag{4}
\end{aligned}$$

The HRS first hyperpolarizability,  $\beta_{\text{HRS}}$ , is given by

$$\beta_{\text{HRS}} = \sqrt{\langle \beta_{ZZZ}^2 \rangle + \langle \beta_{ZXX}^2 \rangle} \tag{5}$$

The depolarization ratio DR is defined as follows:

$$\text{DR} = \frac{\langle \beta_{ZZZ}^2 \rangle}{\langle \beta_{ZXX}^2 \rangle} = \frac{I_{VV}}{I_{HV}} \tag{6}$$

Actually, the DR value depends on the molecular symmetry and can be used to divide up the molecules into three categories based on the shape of the NLO-phore: this ratio ranges from 1.5 to 5 and to 9 for octupolar, one-dimensional/linear push-pull, and dipolar molecules, respectively.<sup>54,107,108</sup> Combining equations 2, 3 and 6, we obtain a simplified expression:

$$C_{\Psi V} = (1 - \text{DR}) \cos^2 \Psi + \text{DR} \tag{7}$$

In terms of molecular quantities, the nonlinear anisotropy,  $\rho$ , corresponds to the ratio between the dipolar ( $|\beta_{J=1}|$ ) and octupolar ( $|\beta_{J=3}|$ ) contributions to the total HRS first hyperpolarizability tensor:

Sample title

$$\rho = \frac{|\beta_{J=3}|}{|\beta_{J=1}|} \quad (8)$$

Note it is also possible to use an equivalent expression to equation 7 using the molecular quantity  $\rho$ :

$$C_{\Psi V} = - \left( \frac{8}{45} + \frac{2}{105} \rho^2 \right) \cos^2 \Psi + \left( \frac{9}{45} + \frac{6}{105} \rho^2 \right) \quad (9)$$

## B. Experimental Methods

HRS measurements were performed using a homemade setup that has been extensively described in previous papers.<sup>109,110</sup> An optical parametric generator (OPG) picosecond laser source (idler: 1150-2200 nm) was used as probing source to adjust the incident energy ( $\omega$ ) to tune the HRS ( $2\omega$ ). The solvents were purchased from sigma-Aldrich with a purity higher than 99.5% (HPLC grade). The di-8-ANEPPS probe was purchased from Merck with a purity of 95% (high-performance liquid chromatography grade) (CAS number 157134-53-7). Disperse red one (DR1), which was used as an external reference molecule for the HRS measurements, was purchased from Aldrich with a purity of 95% (CAS number 2872-52-8). Quartz cells with  $3 \times 3 \text{ mm}^2$  of section were used to minimize the volume to  $\sim 60$  to  $200 \mu\text{l}$  depending on the dilution. The output power of the Near-Infrared (NIR) transmitted incident beam was monitored during all experiments with a calibrated thermal position and power sensors (Thorlabs) so that any spurious data recording could be detected.

Visible absorption spectra of the solutions are reported in Figure 2. The emitted fluorescence of the di-8-ANEPPS is extremely strong in the visible, whatever the solvent considered, so that the scattered photons, in the visible range and picosecond regime, from either two-photon excitation (HRS) or, even more efficiently, three-photon excitation (third harmonic scattering: THS) was at the origin of a secondary one-photon emission fluorescence (see Section S8.1). This secondary emission was so efficient that it was impossible to achieve properly any HRS measurements, even down to the NIR range, at 1700 nm. As a consequence, HRS measurements of ANEPPS had to be performed using a deep-NIR incident excitation, practically beyond 1800 nm. Therefore, critical non-deuterated solvent as ethanol was excluded due to its low transparency in the NIR range. Deuterated chloroform was preferred to chloroform because it is almost transparent in the full range of the OPG laser (1200-2000 nm). NIR spectra of the pure solvents are reported in Fig-

ure S15. So far, this is the first time HRS scattering experiments, in the picosecond regime, are performed in such NIR range and with very moderate average input power ( $\leq 3\text{mW}$ ) so that no spurious effect is triggered, such as electrostriction. A first challenge was to get a good signal-to-noise (SNR) HRS response when selecting an appropriate incident laser wavelength for each solvent so that its absorption loss is as close as possible to zero, avoiding thermal effects. Actually, the absorption of deuterated ethanol (Eth-OD) from 1700 nm to 2000 nm was still too strong (Figure S15) to perform HRS measurements without heating the solution. We restricted our experimental studies to  $\text{DCCl}_3$ , DMF and DMSO, using, respectively, the following set of incident wavelengths (1900 nm, 1950 nm), 1860 nm, and (1840 nm, 1950 nm). The transmission loss of the NIR incident beam for the different experiments are gathered in Table S11. A second challenge was then to select an external reference chromophore since in that deep NIR range, no HRS contribution from the solvent could be measured to achieve the internal reference method. We have selected Disperse Red one (DR1) as an external reference since first, it is a well-known commercial chromophore and second, it exhibits a good signal in the 1200-2000 nm NIR range when solvated in  $\text{DCCl}_3$ . We performed a full analysis of DR1 at 1300 nm and 1500 nm (and a partial check at 1600 nm and 1950 nm), whenever the solvent contribution ( $\text{DCCl}_3$ ) was still measurable as an internal reference<sup>18</sup> (Section S9.2.A - calibration of the external reference DR1). From this, it was possible to extrapolate the frequency dispersion of the external reference<sup>94,111,112</sup> (DR1) in the full NIR range from 1200 to 2000 nm (See Section S9.3 -Extrapolation of the external reference DR1). A description of this original and general procedure is given in the supporting information Section S9.1 - HRS details and method. The concentrations of the various solutions are listed in Table I.

|    | DR1@ $\text{DCCl}_3$  | ANEPPS@ $\text{DCCl}_3$ | ANEPPS@DMSO           | ANEPPS@DMF            |
|----|-----------------------|-------------------------|-----------------------|-----------------------|
| C0 | $1.02 \times 10^{-4}$ | $1.69 \times 10^{-3}$   | $2.37 \times 10^{-3}$ | $5.06 \times 10^{-4}$ |
| C1 | $7.63 \times 10^{-5}$ | $1.26 \times 10^{-3}$   | $1.78 \times 10^{-3}$ | $3.80 \times 10^{-4}$ |
| C2 | $5.09 \times 10^{-5}$ | $8.43 \times 10^{-4}$   | $1.19 \times 10^{-3}$ | $2.53 \times 10^{-4}$ |
| C3 | $2.54 \times 10^{-5}$ | $4.22 \times 10^{-4}$   | $5.93 \times 10^{-4}$ | $1.27 \times 10^{-4}$ |

Table I: Solution concentrations (M) used in the HRS experiments.

## C. Computational and Theoretical Chemistry Methods

### 1. Molecular Dynamics Simulations

The dynamic nature of the solute-solvent system was modeled using Molecular Dynamics (MD) simulations performed with the NAMD code<sup>113</sup> and analyzed with VMD.<sup>114</sup> The cubic boxes (of sides of 70 Å), were created using the Packmol package,<sup>115</sup> each containing one molecule of di-8-ANEPPS and 2900, 4000, 2850, 4500 molecules of solvent for the DCCl<sub>3</sub>, DMSO, DMF, and Eth-OD systems, respectively. An additional DCCl<sub>3</sub> system was created where the molecule of di-8-ANEPPS was replaced by one molecule of DR1. All simulations started from a density close to the experimental one, which are 1.48, 0.79, 0.94, and 1.10 for DCCl<sub>3</sub>, Eth-OD, DMF, and DMSO, respectively.<sup>116</sup> The systems were first equilibrated for 10 ns in the NPT ensemble (P = 1 atm, and T = 298.15 K), before continuing for 50 ns for the production run. The NPT ensemble was maintained using a Nosé-Hoover Langevin piston barostat<sup>117</sup> and a Langevin dynamics thermostat with a coupling constant of 1.0 ps. The Lennard-Jones interactions were truncated using a switching cutoff from 10 Å to 12 Å<sup>118</sup> while the long-range Coulombic interactions were treated using the smooth particle-mesh Ewald (PME) technique.<sup>119</sup> All simulations were performed with a time step of 1 fs. The solvents were simulated using the following force fields (FF): (i) AMBER<sup>120</sup> for DCCl<sub>3</sub>, (ii) GAFF<sup>121</sup> for DMSO and Eth-OD, and (iii) GAFF with charges and nonbonded interactions from Desfrancois *et al.*<sup>122</sup> for DMF. Reparameterized versions of GAFF (rp1GAFF and rp2GAFF) were used for the probe molecules. Both reparameterizations involve fine tuning of the equilibrium bond lengths as well as of some torsion angles, ensuring a better description of the equilibrium geometry. This is crucial since the  $\beta$  responses are highly sensitive to the molecular geometry. To this end, relaxed potential energy scans (PESs) were computed at the M06-2X/cc-pVTZ level on both probes, and fitted using the Adaptive Biasing Force (ABF) procedure.<sup>123</sup> Additionally, the ESP atomic charges are evaluated at the M06-2X/aug-cc-pVTZ level. The rp1GAFF version for di-8-ANEPPS was developed and tested in previous publications (see References<sup>59, 60 and 61</sup>), while the details of the rp2GAFF version for DR1 can be found in the SI.

## 2. Calculations of the First Hyperpolarizability

Calculations of the dynamic NLO responses at various wavelengths were performed at the TDDFT/M06-2X/6-311+G\* level using the Gaussian16 package<sup>124</sup> unless otherwise noted. The M06-2X exchange-correlation functional was demonstrated to perform well at predicting (non)linear optical responses of a variety of chromophores.<sup>125–131</sup> Moreover, as NLO calculations are time-consuming, a small but sufficiently flexible basis set is needed. As shown on azo-type dyes, simple basis sets such as 6-31G\* or 6-31+G\* already provide a good balance between accuracy and computational effort.<sup>132</sup> In the end, the 6-311+G\* basis set was selected, which is routinely used in (non)linear optical property calculations.<sup>16,45,48,65,129,133</sup> Here, we report values of both the HRS responses,  $\beta_{\text{HRS}}$ , and their associated depolarization ratios (DR). The NLO calculations were performed on 50 structures extracted from the MD production run (every 1 ns).

Solvent effects were taken into account using several solvation models: (i) using a continuum embedding through the integral equation formalism (IEF) of the polarizable continuum model (PCM)<sup>134–136</sup> or the Solvation Model Density (SMD)<sup>36</sup> variant. SMD differs from PCM in the choice of atomic radii and the way in which the non-electrostatic (short-range) contribution [the Cavity Dispersion Solvent Structure (CDS) term] is calculated.<sup>36</sup> SMD has been shown to perform better than PCM when computing the free energy of solvation,<sup>36,137,138</sup> or when predicting the absorption spectra of solutes forming intermolecular H-bonds with the solvent. It is also widely used in the field of NLO.<sup>138–141</sup> (ii) using a QM/MM approach, where solvent molecules in close proximity (up to 5.0 Å) to the probe are represented with their point charges while the rest of the bulk is modeled at the IEF-PCM level (EE+PCM). (iii) using a discrete embedding with the Polarizable Embedding (PE)<sup>31,142</sup> as implemented in the Dalton program.<sup>143</sup> In the latter approach, only the chromophore is described at the QM level, while the solvent molecules in a 20.0 Å radius around the chromophore are modeled using the Polarizable Embedding Library. These calculations were performed at the CAM-B3LYP/6-311+G\* level due to implementation limitations on Dalton. The PE Library includes parameters for HCCl<sub>3</sub>, Eth-OH, and DMSO, but not for DMF. Therefore, the atom-centered restrained electrostatic potential (RESP) charges<sup>144</sup> and the atomic isotropic polarizabilities were evaluated following a similar procedure as the one used for PE Library developed by Beerepoot *et. al.*<sup>145</sup> More details and the derived embedding parameters for DMF can be found in SI.

The two-state approximation (TSA)<sup>146</sup> can help rationalizing the  $\beta_{\text{HRS}}$  results by providing

qualitative relationships between the  $\beta_{\text{HRS}}$  responses and simple spectroscopic quantities. It involves the transition dipole between the ground and excited states ( $\mu_{eg}$ ), the difference between the ground and excited state dipole moments ( $\Delta\mu_{eg} = \mu_e - \mu_g$ ), and the corresponding excitation energy ( $\Delta E_{eg} = E_e - E_g$ ), as written in Equation 10. All three spectroscopic quantities, computed at the TDDFT/M06-2X/6-311+G\*, (or CAM-B3LYP/6-311+G\* for PE, level allow to obtain the dominant diagonal tensor component ( $\beta_{zzz}$ ). Then, Equation 11 is needed to convert  $\beta_{zzz}$  into  $\beta_{\text{HRS}}$ , assuming the other components are negligible.

$$\beta_{zzz} = 6 \frac{\mu_{eg}^2 \Delta\mu_{eg}}{\Delta E_{eg}^2} \quad (10)$$

$$\beta_{\text{HRS TSA}} = \sqrt{\frac{6}{35}} \beta_{zzz} \quad (11)$$

### 3. Configuration Sampling and its Analysis

The importance of the configuration sampling obtained via MD simulations is evident when considering the distribution of both the linear and nonlinear optical responses obtained for the probes in different solvents. For the linear properties, the simulated UV/Vis absorption spectra are displayed in Figures S7-S10. They are obtained from distributions of the lowest-energy dipole-allowed excitation energies and oscillator strengths. Also, the standard deviations of the average TDDFT vertical excitation energies ( $\Delta E^{\text{vert}}$ ) values (Figure S6), represent  $\sim 5\%$  of the average  $\Delta E^{\text{vert}}$  values. For  $\beta_{\text{HRS}}$ , the statistical analysis over the 50 snapshots yields a standard deviation that represents 5-25% of the average. Although the individual values vary, the cumulative averages converge quickly ensuring 50 snapshots are enough to describe the  $\beta_{\text{HRS}}$  response of the systems. (Figures S28-S36). However, identical  $\beta_{\text{HRS}}$  mean values and standard deviations are sometimes associated with different distribution profiles (Figures S37-S42). This can be seen by comparing the distribution profiles of ANEPPS@DCCl<sub>3</sub> obtained using PCM or SMD (Figures S37a and S37d, respectively). Note that the distribution profiles are also affected by changing the incident wavelength, as shown in the calculations at 1900 nm and 1950 nm for ANEPPS@DCCl<sub>3</sub> and 1840 nm and 1950 nm for ANEPPS@DMSO. Although this does not affect the resulting averages and standard deviations much. All of this highlights the importance of taking into account the dynamical nature of the solvents.

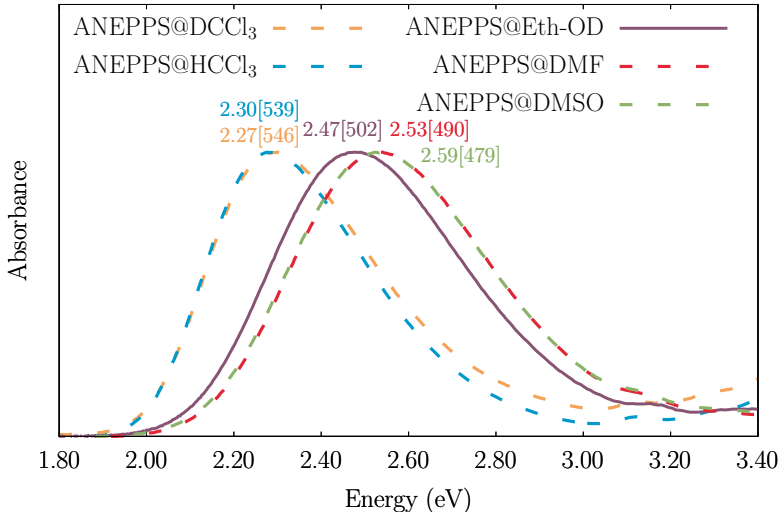


Figure 2: Normalized experimental UV/Vis absorption spectra of di-8-ANEPPS in  $\text{DCCl}_3$ ,  $\text{HCCl}_3$ , Eth-OD, DMF, and DMSO. The experimental maximum absorption energies,  $\Delta E^{max}$  (eV), and wavelengths [ $\lambda^{max}$ , nm] are superimposed to the curves.

### III. RESULTS AND DISCUSSION

#### A. Linear Optical Responses

The UV/Vis absorption spectrum of di-8-ANEPPS (Figure 2) exhibits the conventional blue shift of hemicyanines when increasing the solvent polarity,<sup>147–150</sup> going from ANEPPS@ $\text{DCCl}_3$  to ANEPPS@DMSO. This is quantified using the solvent polarity indicator ( $E_T^N$ ) of Reichardt,<sup>151</sup> showing, for aprotic solvent, a good linear relationship with the experimental absorption maximum,  $\Delta E^{max}$ , as shown in Table S7 and Figure S5. This Table also reveals that experimental trend is well reproduced by TDDFT calculations with the different solvation models. Yet, the slope of the linear regressions are underestimated with respect to the experiment.

Interestingly, Fromherh *et. al*<sup>152</sup> showed that the solvatochromism of these cationic dyes (the sulfonate group being not involved in the  $\pi$ -conjugated frame) is quite unusual. Their absorption and emission spectra reveal a striking symmetry: the absorption spectrum is blue-shifted, while the emission spectrum is red-shifted, as is also observed here (Table S10), by an almost identical energy when the solvent polarity increases. It was latter reported in other works<sup>148,153–156</sup> and studies have focused on rationalizing this uncommon solvatochromism.<sup>157</sup> Usually, the solvatochromism experienced by the probe is explained by comparing the ground ( $\mu_g$ ) and excited ( $\mu_e$ ) dipole moments at a given equilibrium geometry.<sup>158</sup> If, assuming an instantaneous transition,

the dipole moment increases upon excitation, the excited state,  $e$ , gets more stabilized by the solvation than the ground state,  $g$ , and the energy gap ( $\Delta E_{eg}$ ) between the two states decreases with the solvent polarity. This corresponds to a red shift of both the absorption and emission spectra. On the contrary, if the dipole moment decreases, the absorption and emission spectra are blue-shifted. In both cases, the magnitude of the shift is influenced by the  $\Delta\mu_{eg}$  difference. For di-8-ANEPPS, the photo-induced electronic reorganization results in the transfer of the effective positive charge from the pyridinium to the amino-naphthalene,<sup>147</sup> as shown by the representation of the pair of orbitals involved in the transition (Figures 3a and 3b), as well as by the charge transfer vector (Figure 3e and Table S9). The charge transfer vector represents the distance between the baricenters associated with the increase and decrease of the electronic density upon excitation. This electronic redistribution foresees a transition from the benzenoid to the quinoid forms (Figures 3c and 3d). These valence-bond (VB) forms are also associated with resonance structures of the ground state.<sup>147,149</sup> Since the charges, carried by the sulfonate and the amino-naphthalene are farther apart in the excited state, the dipole moment gets larger (Table S8). In the two VB state formulation, this should result in a red shift of both the absorption and emission spectra in more polar solvents. However, this is not what is observed in this work and previous experimental reports<sup>148,153–156</sup> nor what is observed here. This unusual solvatochromism is explained by the balance between two contributions: (i) the electronic energy difference between the equilibrated ground and excited states,  $\Delta E_{eg}^{elec}$ , and (ii) the solvent reorganization energy in the excited (ground) state,  $\Lambda_s^e$  ( $\Lambda_s^g$ ), such that the absorption and emission processes are governed by:

$$\Delta E_{eg}^{abs} = \Delta E_{eg}^{elec} + \Lambda_s^e \quad (12)$$

$$\Delta E_{eg}^{em} = \Delta E_{eg}^{elec} - \Lambda_s^g \quad (13)$$

In more polar solvents, both  $\Lambda_s^e$  and  $\Lambda_s^g$  increase. As a consequence, the Stokes shift,  $\Delta E_{eg}^{abs} - \Delta E_{eg}^{em}$ , increases also, as shown in Table S10. Furthermore,  $\Delta E_{eg}^{elec}$  is also affected and tends to shift both the absorption and emission spectra in the same direction (*i.e.* no modification of the Stokes shift). For "normal" push-pull polyenes, the effect on  $\Delta E_{eg}^{elec}$  is dominant and shifts both the absorption and emission spectra in the same direction, while for hemicyanines, the contribution from the solvent reorganization energy is dominant. Therefore, the absorption (emission) spectrum is blue-(red-)shifted upon increasing the solvent polarity.

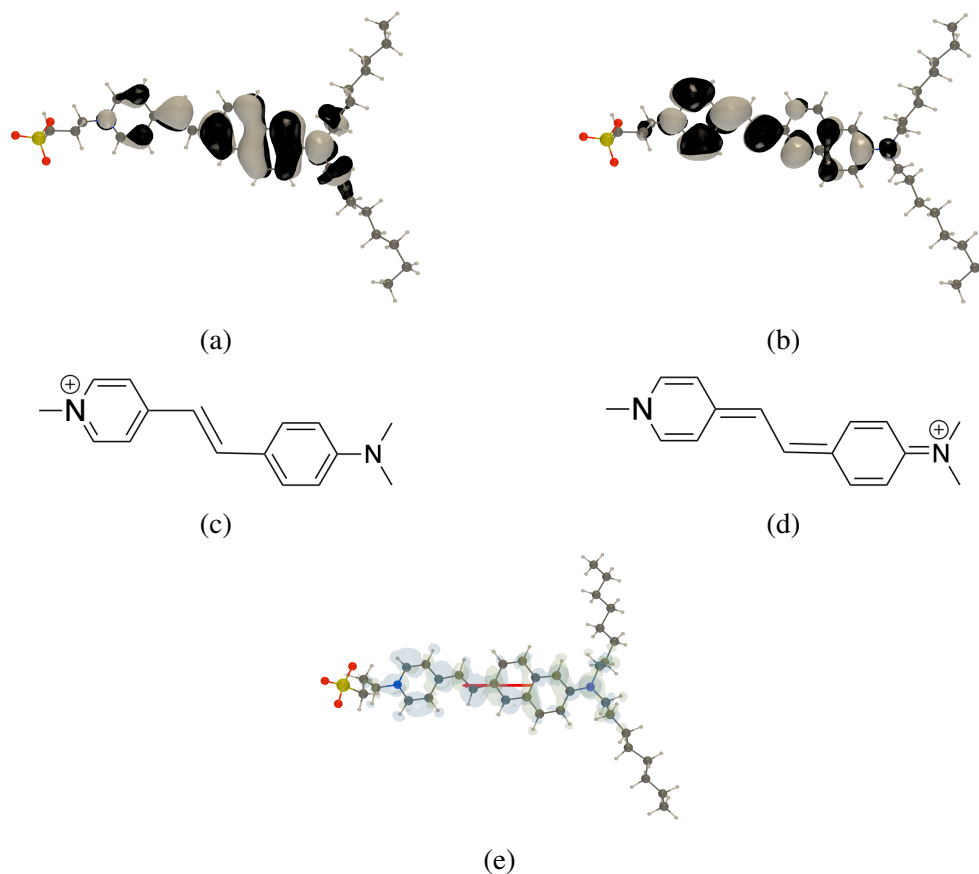


Figure 3: Representation of the molecular orbitals involved in the lowest-energy transition computed at the TDDFT/M06-2X/6-311+G\*/PCM level for ANEPPS@DCCl<sub>3</sub>: **(a)** highest occupied molecular orbital (HOMO), and **(b)** lowest unoccupied molecular orbital (LUMO). Resonance structures of the hemicyanine cationic core of the di-8-ANEPPS dye: **(c)** benzenoid form and **(d)** quinoid form. **(e)** charge transfer vector [red] between the barycenters of the positive and the negative densities.

Regarding the ability of theoretical models to reproduce solvent effects, Table II presents the experimental maximum absorption energies ( $\Delta E^{max}$ ), and the calculated vertical excitation energies ( $\Delta E^{vert}$ ) and associated oscillator strengths ( $f$ ). Keeping in mind that these quantities are different in nature, we observe that  $\Delta E^{vert}$  is systematically larger than  $\Delta E^{max}$  (see also Figure S6).<sup>159,160</sup> Indeed, TDDFT studies have found gaps between the vertical and maximum absorption  $\Delta E$  values in the 0.13-0.23 eV range for cyanine dyes, depending on the system and the level of theory.<sup>161-164</sup> We want to stress that the PE results obtained at the CAM-B3LYP/6-311+G\* level are very similar to those obtained with PCM/SMD using the M06-2X/6-311+G\* level. The oscillator strengths (in the 1.50-1.70 range) predicted by all models are very close and vary by at most  $\sim 10\%$  for each solvent. With SMD and PE, the  $f$  values are systematically the largest,

while EE+PCM produces the smallest ones. The focus here is to assess whether the solvation models are able to reproduce the variations of  $\Delta E^{max}$  observed between the four solvents. Taking the results in  $\text{DCCl}_3$  as reference, the experimental UV/Vis absorption spectrum is blue-shifted by 0.20 eV ( $\sim 0.27$  eV) going from  $\text{DCCl}_3$  to Eth-OD (DMF, DMSO). The continuum models, PCM and SMD, display a poor capacity to retrieve the whole  $\Delta E^{max}$  variations, though the trends are correct. Using PCM, the average  $\Delta E^{vert}$  values vary by no more than 0.05 eV for all solvents, while SMD performs slightly better. However, by considering solvent molecules in a sphere of 3.0 Å around the chromophore and describing these by point charges, quantitative agreement is almost reached. Note that no significant improvement is found when enlarging the radius of the explicit solvent spheres to 5.0 Å but these results indicate that the description of the solvent must include a point charge embedding to describe the linear response of cyanine dyes. Then, the more elaborate polarizable embedding (PE) scheme is also shown to be suitable for reproducing the experimental variations in  $\Delta E^{max}$ , but predicts slightly smaller  $\Delta E^{vert}$  variations than EE+PCM.

To gain deeper insight on solvent effects, it is also helpful to look at the variation of  $\Delta E^{vert}$  when going from the isolated gas phase to the solutions (Table S6). Starting from  $\Delta E_{gas}^{vert} = 2.82$  eV, including the environment creates a red shift in the absorption spectra, consistent with what is observed when increasing the solvent polarity. The largest bathochromic shift is obtained for  $\text{DCCl}_3$ , regardless of the solvation model, and decreases with solvent polarity. On the other hand, the amplitude of bathochromism depends on the solvation model. This can be explained when looking at the total electronic energies (Figure S12): (i) strict continuum models (PCM and SMD) predict a destabilization of both the ground and excited states compared to the gas phase situation, but since  $g$  is more destabilized than  $e$ , it results in a red shift. (ii) QM/MM models such as EE+PCM predict a stabilization of both  $g$  and  $e$  upon solvation. However, since  $e$  is more stabilized than  $g$ , it also results in a bathochromic shift. Finally, (iii) the PE results fall into either the (i) or (ii) situation. This means that the  $g$  and  $e$  are either both stabilized (DMF and DMSO) or destabilized ( $\text{DCCl}_3$  and Eth-OD), yielding for all solvents a  $\Delta E_{eg}$  smaller than in the gas phase. In all cases, a substantial negative solvatochromism is observed, showing the solvent ability to tune the linear optical responses.

|                 | ANEPPS@DCCl <sub>3</sub> |             | ANEPPS@EthOD |             | ANEPPS@DMF  |             | ANEPPS@DMSO |             |
|-----------------|--------------------------|-------------|--------------|-------------|-------------|-------------|-------------|-------------|
|                 | $\Delta E$               | $f$         | $\Delta E$   | $f$         | $\Delta E$  | $f$         | $\Delta E$  | $f$         |
| Exp.            | 2.30 <sup>1</sup> , 2.27 | -           | 2.47         | -           | 2.54        | -           | 2.53        | -           |
| PCM             | 2.56 ± 0.09              | 1.66 ± 0.11 | 2.60 ± 0.11  | 1.70 ± 0.15 | 2.59 ± 0.10 | 1.68 ± 0.11 | 2.61 ± 0.12 | 1.64 ± 0.13 |
| EE3+PCM         | 2.53 ± 0.08              | 1.59 ± 0.12 | 2.64 ± 0.12  | 1.51 ± 0.14 | 2.69 ± 0.10 | 1.66 ± 0.10 | 2.67 ± 0.14 | 1.56 ± 0.14 |
| EE5+PCM         | 2.53 ± 0.08              | 1.59 ± 0.12 | 2.66 ± 0.12  | 1.51 ± 0.13 | 2.69 ± 0.10 | 1.66 ± 0.10 | 2.68 ± 0.12 | 1.55 ± 0.14 |
| SMD             | 2.57 ± 0.12              | 1.72 ± 0.15 | 2.65 ± 0.12  | 1.72 ± 0.14 | 2.66 ± 0.11 | 1.71 ± 0.10 | 2.68 ± 0.13 | 1.67 ± 0.12 |
| PE <sup>2</sup> | 2.55 ± 0.09              | 1.67 ± 0.12 | 2.63 ± 0.11  | 1.70 ± 0.15 | 2.66 ± 0.12 | 1.72 ± 0.10 | 2.68 ± 0.16 | 1.67 ± 0.13 |

Table II: Di-8-ANEPPS experimental maximum absorption energies ( $\Delta E^{max}$ ) (eV) and averaged vertical transition energies ( $\Delta E^{vert}$ ) (eV) and their associated oscillator strengths ( $f$ ), as well as standard deviations calculated at the TDDFT/M06-2X/6-311+G\* level with different solvation models. <sup>1</sup>Results for ANEPPS@HCCl<sub>3</sub> <sup>2</sup>The PE results were obtained at the CAM-B3LYP/6-311+G\* level.

## B. Nonlinear Optical Responses

The measured first hyperpolarizability values,  $\beta_{\text{HRS}}^{exp}$ , are listed in Table III (see Table S13 for details). The corresponding power scans and polarization scans are given in Figures S21-S25. All experimental values are in the  $20\text{-}35 \times 10^3$  a.u. range and decrease when increasing the solvent polarity. In fact, a good correlation is observed between  $\beta_{\text{HRS}}$  and the reverse solvent polarity indicator  $(E_T^N)^{-1}$  (Figure S26), which is qualitatively consistent with the global linear behavior of  $\Delta E_{eg}$  ( $\Delta E^{max}$ ) with  $E_T^N$ . Note that using the TSA, displayed at Equation 10, a  $(E_T^N)^{-2}$  dependence is predicted if the terms in the numerator is independent of the solvent. Still, a good correlation is obtained between  $\beta_{\text{HRS}}$  and  $(E_T^N)^{-2}$  (Figure S27).

The TDDFT  $\beta_{\text{HRS}}$  values,  $\beta_{\text{HRS}}^{th}$ , systematically overestimate the experimental data as  $\beta_{\text{HRS}}^{th}$  lie in the  $30\text{-}50 \times 10^3$  a.u. range. Across all models, the smallest errors are found for the ANEPPS@DCCl<sub>3</sub> system (overestimation of  $\sim 30\%$ ), then the difference between  $\beta_{\text{HRS}}^{exp}$  and  $\beta_{\text{HRS}}^{th}$  increases with the solvent polarity. PCM always predicts the largest  $\beta_{\text{HRS}}^{th}$  response, with values up to twice as large as the measured ones. Taking into account a charge embedding around the probe, the  $\beta_{\text{HRS}}^{th}$  values are  $\sim 10\%$  ( $\sim 20\%$ ) smaller than when using PCM alone for ANEPPS@DCCl<sub>3</sub>(DMF, DMSO). The less polar DCCl<sub>3</sub> system is less affected by the change in embedding, showing the same results when increasing the number of point charges. This is also the case for ANEPPS@DMF, while for ANEPPS@DMSO the larger embedding hardly reduces  $\beta_{\text{HRS}}^{th}$  further. The other continuum model, SMD, behaves similarly to PCM, but produces slightly smaller results. Finally, using the PE solvation model, the probe exhibits NLO responses

Sample title

between those predicted by the strict continuum models and EE+PCM schemes. Yet, the results obtained using PE and CAM-B3LYP/6-311+G\* are very similar to those obtained using M06-2X/6-311+G\*/PCM.

|                      | ANEPPS@DCCl <sub>3</sub> |             | ANEPPS@Eth-OD | ANEPPS@DMF  |                   | ANEPPS@DMSO |                   |             |
|----------------------|--------------------------|-------------|---------------|-------------|-------------------|-------------|-------------------|-------------|
|                      | 1900                     | 1950        | 1900          | 1860        | 1900 <sup>1</sup> | 1840        | 1900 <sup>1</sup> | 1950        |
| $\beta_{\text{HRS}}$ |                          |             |               |             |                   |             |                   |             |
| Exp.                 | 33                       | 32          | -             | 23          | 23                | 21          | 21                | 21          |
| PCM                  | 46 ± 6                   | 45 ± 6      | 43 ± 7        | 45 ± 7      | 44 ± 7            | 43 ± 8      | 42 ± 8            | 41 ± 7      |
| EE3+PCM              | 41 ± 5                   | 40 ± 5      | 34 ± 7        | 36 ± 5      | 35 ± 5            | 34 ± 7      | 33 ± 7            | 32 ± 7      |
| EE5+PCM              | 41 ± 5                   | 40 ± 4      | 33 ± 6        | 36 ± 5      | 35 ± 5            | 33 ± 6      | 32 ± 6            | 31 ± 6      |
| SMD                  | 46 ± 7                   | 44 ± 7      | 40 ± 7        | 42 ± 7      | 41 ± 7            | 40 ± 8      | 39 ± 8            | 38 ± 8      |
| PE <sup>2</sup>      | 44 ± 5                   | 43 ± 5      | 38 ± 8        | 37 ± 7      | 36 ± 7            | 37 ± 9      | 36 ± 9            | 35 ± 8      |
| DR                   |                          |             |               |             |                   |             |                   |             |
| Exp.                 | 3.04                     | 2.65        | -             | 2.80        |                   | 3.51        |                   | 2.94        |
| PCM                  | 4.91 ± 0.02              | 4.91 ± 0.02 | 4.92 ± 0.01   | 4.92 ± 0.01 |                   | 4.91 ± 0.02 |                   | 4.91 ± 0.02 |
| EE3+PCM              | 4.90 ± 0.04              | 4.90 ± 0.04 | 4.91 ± 0.02   | 4.90 ± 0.02 |                   | 4.90 ± 0.02 |                   | 4.90 ± 0.03 |
| EE5+PCM              | 4.90 ± 0.04              | 4.89 ± 0.04 | 4.91 ± 0.02   | 4.90 ± 0.02 |                   | 4.90 ± 0.03 |                   | 4.89 ± 0.03 |
| SMD                  | 4.91 ± 0.02              | 4.90 ± 0.02 | 4.91 ± 0.01   | 4.91 ± 0.01 |                   | 4.91 ± 0.02 |                   | 4.90 ± 0.02 |
| PE <sup>2</sup>      | 4.91 ± 0.01              | 4.91 ± 0.01 | 4.89 ± 0.03   | 4.89 ± 0.04 |                   | 4.89 ± 0.03 |                   | 4.89 ± 0.03 |

Table III: Di-8-ANEPPS experimental ( $\beta_{\text{HRS}}^{\text{exp}}$ ) and calculated ( $\beta_{\text{HRS}}^{\text{th}}$ ) first hyperpolarizabilities ( $10^3$  a.u.), as well as experimental ( $\text{DR}^{\text{exp}}$ ) and calculated ( $\text{DR}^{\text{th}}$ ) depolarization ratios. <sup>1</sup> $\beta_{\text{HRS}}^{\text{exp}}$  and  $\beta_{\text{HRS}}^{\text{th}}$  values extrapolated at 1900 nm using the TSA. <sup>2</sup>The PE results were obtained at the CAM-B3LYP/6-311+G\* level.

Besides the comparison between individual values, the most important question remaining is whether the theoretical calculations are able to reproduce the variations of the measured NLO responses, and which model performs the best? Among the continuum models, SMD clearly reproduces the variations of the experimental values better than PCM, as shown in Figure 4 (the slope amounts to  $\simeq 1/2$  versus  $1/4$  and  $R^2$  is larger). Then, when adding a point charge embedding (EE+PCM) the variations of the experimental NLO responses are better described (slope of  $\simeq 0.6 - 0.7$  and  $R^2 > 0.9$ ). Adding point charges as well as atomic polarizabilities to the solvent description further improves the correlation between  $\beta_{\text{HRS}}^{\text{th}}$  and  $\beta_{\text{HRS}}^{\text{exp}}$  ( $R^2 = 0.97$ ).

Regarding DR values (Table III), the measured ones are in the 2.6-3.5 range and, contrary to  $\beta_{\text{HRS}}^{\text{exp}}$ , the changes between solutions cannot be related to the increase in the solvent polarity.  $\text{DR}^{\text{exp}}$  is also affected by the incident wavelength, but the responses for all systems are not changing in the same way. For ANEPPS@DCCl<sub>3</sub>, increasing the incident wavelength from 1900 nm to

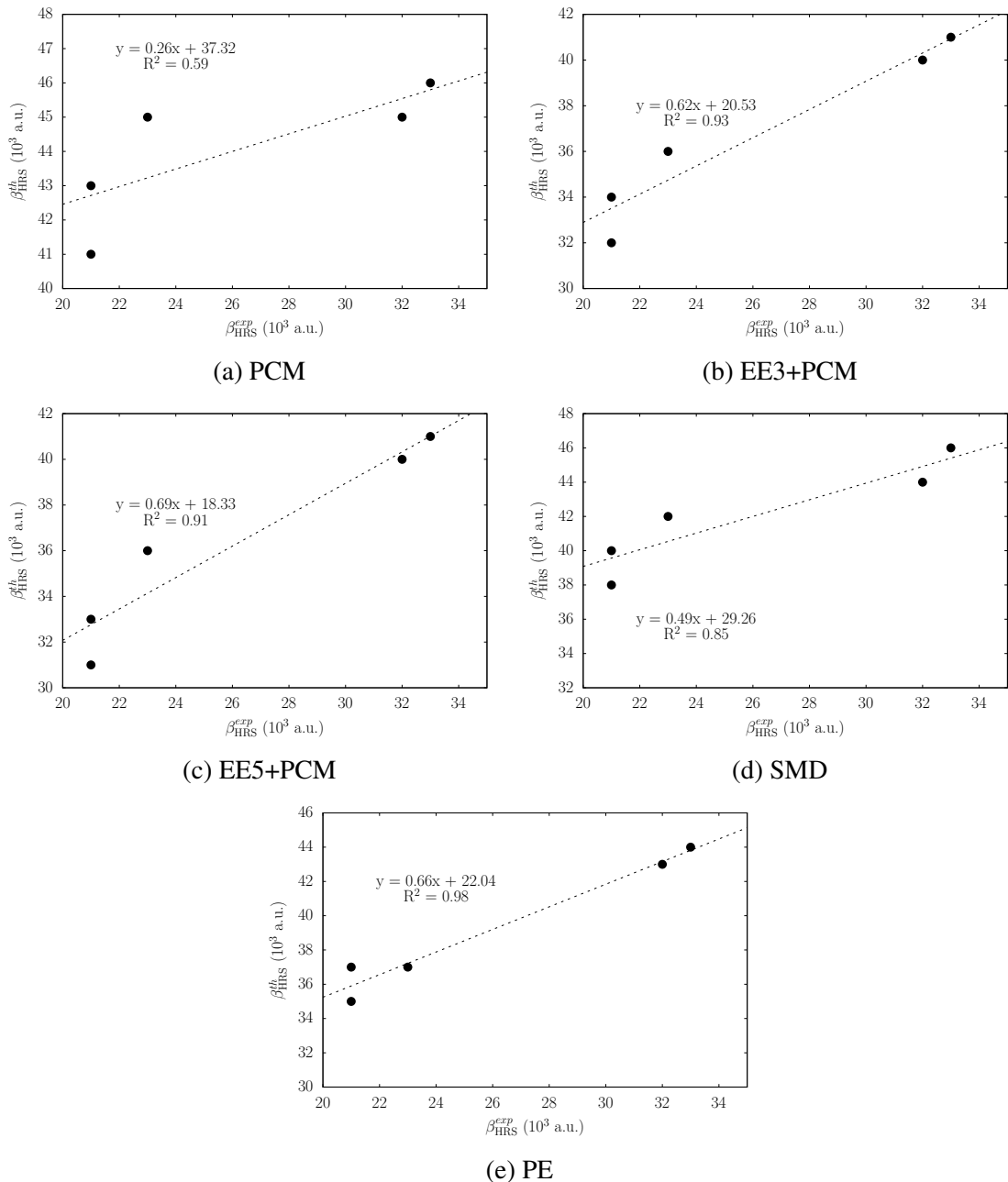


Figure 4: Calculated first hyperpolarizabilities ( $\beta_{\text{HRS}}^{\text{th}}$ ) as a function of the experimental first hyperpolarizabilities ( $\beta_{\text{HRS}}^{\text{exp}}$ ) ( $10^3$  a.u.).

1950 nm decreases DR from  $3.04 \pm 0.35$  to  $2.65 \pm 0.16$ . Reversely, when increasing the incident wavelength in the case of ANEPPS@DMSO, the DR increases from  $2.65 \pm 0.32$  to  $2.95 \pm 0.24$ . Moreover, the standard deviations associated with those values are quite high (from 8-25% of the average value), especially for ANEPPS@DMF for which the DR amounts to  $2.80 \pm 0.72$ . Even considering those standard deviations, calculations overestimate the DR values.  $\text{DR}^{\text{th}}$  are all close

to 5, characteristic of push-pull molecules, and are hardly affected by changes in the environment or the way it is taken into account, or even the incident wavelength. The standard deviations are quite small and the associated distribution profiles are narrow (Figures S42-S51), regardless of the system or solvent model.

We should stress here that the variations of  $\beta_{\text{HRS}}^{\text{th}}$  observed between the different solvents are not caused by changes in the geometry of the probe. The geometry of the chromophore is barely impacted by its environment. For this analysis, two key parameters were considered: the torsion angles and the bond length alternation (BLA) computed along the conjugated path between the aromatic cycles (see Table S4 for the parameters definition). As seen in Figures S3 and S4 and Table S4, even though there are slight differences in the distribution profiles, the average parameters do not change from one system to the next: all torsion angles present an out-of-plane distortion of about  $10^\circ$  in all solvents, while the BLA remains at  $0.06 \pm 0.03 \text{ \AA}$ .

Finally, more reliable analyses of the solvent effects can be achieved when comparing the NLO responses all collected at the same incident wavelength. Using the TSA, the experimental and calculated results for DMF and DMSO obtained at 1860 nm or 1950 nm were converted to their corresponding responses at 1900 nm. At this wavelength, the  $\beta_{\text{HRS}}$  values of both ANEPPS@DMF and ANEPPS@DMSO are nearly identical (within the experimental precision and the calculated standard deviation).

### C. Linear and Nonlinear Optical Responses of DR1

As mentioned above, DR1 is often used as an external reference in HRS experiments and it is preferred to another commonly used probe,<sup>94,111,165–168</sup> PNA, when investigating NLO responses in the long wavelengths regime. Here, DR1 was used as a reference in the HRS measurements of di-8-ANEPPS because it does not show fluorescence at these long wavelengths.<sup>87,88,90</sup> While a number of works have reported calculated  $\beta$  of PNA,<sup>20,169–172</sup> very few studies have focused on the theoretical characterization of DR1. The aim of this Section is therefore to discuss the NLO responses of DR1 in more detail and to compare a new set of experimental data with values calculated using the different solvation models, employed for di-8-ANEPPS.

Table IV lists the experimental maximum absorption energy,  $\Delta E^{\text{max}}$ , and the calculated vertical excitation energy,  $\Delta E^{\text{vert}}$ , of DR1 in  $\text{DCCl}_3$ . Experimentally, DR1 exhibits a maximum of absorption at 2.59 eV. Depending on the solvation model,  $\Delta E^{\text{vert}}$  values range between 2.62 eV

Sample title

and 2.48 eV. So, in contrast to di-8-ANEPPS, continuum models underestimate  $\Delta E_{eg}$ , respectively by 0.07 eV and 0.11 eV for PCM and SMD. The same can be said for PE. On the contrary, when using EE+PCM, the TDDFT vertical excitation energies are slightly larger than the experimental  $\Delta E^{max}$ . Going from the gas phase, where  $\Delta E_{gas}^{vert} = 3.32$  eV, to the  $DCCl_3$  solution produces a red shift in the absorption spectrum, as was observed for the ANEPP dye. As shown in Figure 5, the electronic density is transferred from the amino-benzene to the nitro group upon excitation, producing a larger dipole moment in the excited state than in the ground state (Table S8). Following the two VB state approach discussed above, an increase in dipole moment upon excitation leads, when increasing the solvent polarity, to a red shift of the main absorption band, as is observed by Zakerhamidi *et. al.*<sup>173</sup>

|         | $\Delta E$      | $f$             | $\beta_{HRS}$ |             |             | DR              |                 |                 |
|---------|-----------------|-----------------|---------------|-------------|-------------|-----------------|-----------------|-----------------|
|         |                 |                 | 1300          | 1500        | 1600        | 1300            | 1500            | 1600            |
| Exp.    | 2.59            | -               | 20            | 20          | 19          | 5.03            | 3.72            | 3.70            |
| PCM     | $2.52 \pm 0.17$ | $0.76 \pm 0.16$ | $27 \pm 11$   | $20 \pm 10$ | $21 \pm 13$ | $4.89 \pm 0.73$ | $4.86 \pm 0.74$ | $4.97 \pm 0.59$ |
| EE3+PCM | $2.62 \pm 0.16$ | $0.70 \pm 0.16$ | $17 \pm 6$    | $13 \pm 7$  | $12 \pm 6$  | $4.91 \pm 0.71$ | $4.84 \pm 0.82$ | $4.88 \pm 0.82$ |
| EE5+PCM | $2.62 \pm 0.16$ | $0.70 \pm 0.17$ | $17 \pm 7$    | $13 \pm 7$  | $13 \pm 6$  | $4.91 \pm 0.71$ | $4.81 \pm 0.89$ | $4.90 \pm 0.79$ |
| SMD     | $2.48 \pm 0.17$ | $0.77 \pm 0.15$ | $32 \pm 20$   | $24 \pm 15$ | $23 \pm 24$ | $4.86 \pm 0.72$ | $4.90 \pm 0.62$ | $4.95 \pm 0.61$ |
| PE      | $2.56 \pm 0.16$ | $0.61 \pm 0.16$ | $23 \pm 15$   | $21 \pm 15$ | $18 \pm 9$  | $4.85 \pm 0.75$ | $5.00 \pm 0.58$ | $4.93 \pm 0.70$ |

Table IV: DR1@ $DCCl_3$  (i) experimental maximum absorption energies ( $\Delta E^{max}$ ) (eV) and averaged vertical transition energies ( $\Delta E^{vert}$ ) (eV) and their associated oscillator strengths ( $f$ ), as well as standard deviations calculated at the TDDFT/M06-2X/6-311+G\* level with different solvation models. (ii) experimental ( $\beta_{HRS}^{exp}$ ) and calculated ( $\beta_{HRS}^{th}$ ) first hyperpolarizabilities ( $10^3$  a.u.) at various wavelengths (nm). (iii) experimental ( $DR^{exp}$ ) and calculated ( $DR^{th}$ ) depolarization ratios.

The NLO responses are barely affected by the variation of the incident light from 1300 nm to 1600 nm, and the  $\beta_{HRS}^{exp}$  responses stay at a value around  $20 \times 10^3$  a.u. (see Table IV and Table S12 for further details).  $\beta_{HRS}$  values calculated using the different solvation schemes are either smaller or larger than the experimental ones, depending on the model. As for di-8-ANEPPS, continuum models always predict the largest  $\beta_{HRS}$  values (*i.e.* with the largest overestimations). This is true for SMD over the entire wavelength range. For PCM, the  $\beta_{HRS}$  response is only larger at 1300 nm ( $27 \times 10^3$  a.u.), and nearly identical to the experimental data at 1500 nm and 1600 nm. Adding a discrete charge embedding reduces the PCM values by about 30-40%, and provides values slightly smaller than the measured ones. Finally, by employing the PE scheme, intermediate values are obtained, which show by far the best correlation with the experimental

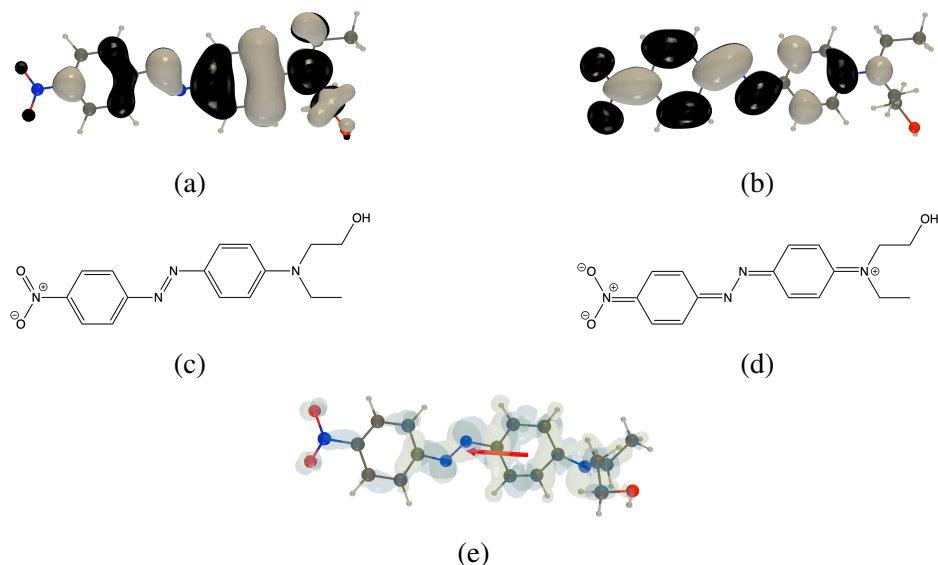


Figure 5: Representation of the molecular orbitals involved in the lowest-energy transition computed at the TDDFT/M06-2X/6-311+G\*/PCM level for DR1@DCCl<sub>3</sub>: **(a)** highest occupied molecular orbital (HOMO), and **(b)** lowest unoccupied molecular orbital (LUMO). **(c)** and **(d)** resonance structures of DR1. **(e)** charge transfer vector [red] between the barycenters of the positive and the negative densities.

data. Indeed, the difference in the performance of the solvation models for predicting the NLO properties of DR1 is quite large. Still, all models anticipate a larger variation of  $\beta_{\text{HRS}}^{\text{th}}$  depending on the incident wavelength than what is observed experimentally.

The  $\beta_{\text{HRS}}^{\text{exp}}$  and  $\beta_{\text{HRS}}^{\text{th}}$  results presented in this work are in the same range as experimental or calculated  $\beta_{\text{HRS}}$  values for DR1 from the literature (Figure 6 and Table V). Values varying between  $9 \times 10^3$  a.u. and  $36 \times 10^3$  a.u. are found, with the exception of the value of  $89 \times 10^3$  a.u. obtained by Makowska-Janusik *et. al.*<sup>174</sup> with a method known to overestimate the NLO responses.<sup>175,176</sup> Particularly, the EE+PCM  $\beta_{\text{HRS}}^{\text{th}}$  values (1300 nm, 1500 nm, and 1600 nm) are in good agreement with the work of Campo *et. al.*<sup>93</sup>

#### D. $\beta_{\text{HRS}}$ using the two-state approximation

It is interesting to check whether the solvent effects, as determined at the TDDFT level, can be reproduced with the TSA, allowing therefore to associate the  $\beta_{\text{HRS}}$  variations with those of simple spectroscopic quantities. First, considering all solvent models, Table ?? show that, for both di-8-ANEPPS and DR1, the  $\beta_{\text{HRS}}$  calculated using the TSA ( $\beta_{\text{HRS TSA}}$ ) are of the same order of magnitude as the full TDDFT ones. However, the  $\beta_{\text{HRS TSA}}$  results do not systematically follow

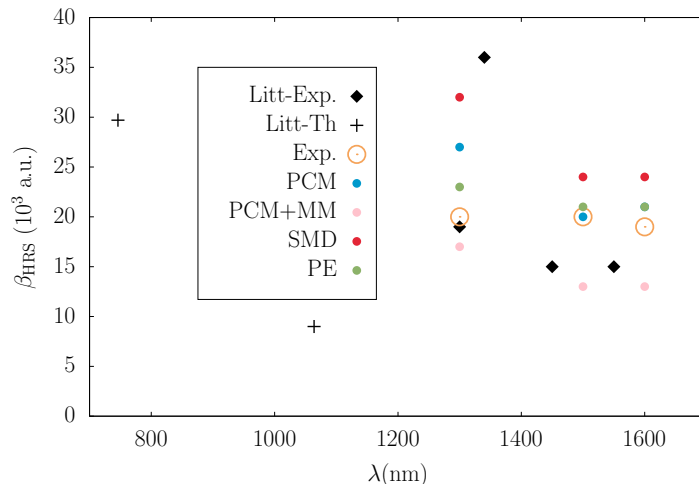


Figure 6:  $\beta_{\text{HRS}}^{\text{exp}}$  and  $\beta_{\text{HRS}}^{\text{th}}$  values ( $10^3$  a.u.) for DR1 from this work compared to data found in the literature. For clarity purposes, the value at 746nm has been divided by 3. Individual values with references can be found in Table V. The orange cross correspond to the  $\beta_{\text{HRS}}^{\text{exp}}$  value extrapolated at 1900 nm.

| Ref.           | Solvent           | $\lambda$ (nm) | Measure  | Convention | Reference   | $\beta_{\text{HRS}}$  |
|----------------|-------------------|----------------|--|------------|---|-----------------------|
| 93             | CHCl <sub>3</sub> | 1300           | $\beta_{\text{zzz}}^{\text{eff}} = 398 \times 10^{-30}$ esu <sup>1</sup> | T          | CHCl <sub>3</sub> : $\beta_{\text{zzz}}^{\text{eff}} = 0.446 \times 10^{-30}$ esu | $19 \times 10^3$ a.u. |
| 93             | CHCl <sub>3</sub> | 1450           | $\beta_{\text{zzz}}^{\text{eff}} = 317 \times 10^{-30}$ esu <sup>1</sup> | T          | CHCl <sub>3</sub> : $\beta_{\text{zzz}}^{\text{eff}} = 0.446 \times 10^{-30}$ esu | $15 \times 10^3$ a.u. |
| 93             | CHCl <sub>3</sub> | 1550           | $\beta_{\text{zzz}}^{\text{eff}} = 302 \times 10^{-30}$ esu <sup>1</sup> | T          | CHCl <sub>3</sub> : $\beta_{\text{zzz}}^{\text{eff}} = 0.446 \times 10^{-30}$ esu | $15 \times 10^3$ a.u. |
| 13             | CHCl <sub>3</sub> | 1340           | $\beta_{\text{HRS}} = 78 \times 10^{-30}$ esu                            | X          | CHCl <sub>3</sub> : $\beta_{\text{HRS}} = 0.26 \times 10^{-30}$ esu               | $36 \times 10^3$ a.u. |
| Ref.           | Solvent           | $\lambda$ (nm) | Calculation  | Convention | Method  | $\beta_{\text{HRS}}$  |
| <sup>174</sup> | isolated          | 746            | $\beta_{\text{HRS}} = 16 \times 10^3$ a.u.                               | B          | PBE/TZ2P  | $89 \times 10^3$ a.u. |
| <sup>177</sup> | isolated          | 1064           | $\beta_{\text{HRS}} = 73 \times 10^{-30}$ esu                            | B          | HF/6-31G*   | $9 \times 10^3$ a.u.  |

Table V: Measured or calculated HRS first hyperpolarizability values for DR1 from the literature.  
<sup>1</sup>Taken from the digitalization of Figure 6 in the article.

every solvent-induced variations seen with TDDFT. Particularly, when using PCM, the TSA does not predict a decrease of the  $\beta$  responses of di-8-ANEPPS in solvent of increasing polarity, as is observed with the other models as well as for the  $\beta_{\text{HRS}}$  TDDFT data (Figure ??). Figure ?? presents the linear regression between the two sets of data. A global correlation coefficient of 0.63 is obtained, but all solvent schemes do not behave the same. Table ?? shows that the largest R<sup>2</sup> coefficient is found with SMD (R<sup>2</sup> = 0.95). Note also that the slope of the relationship are in the 1.0-1.3 range for all solvation models except PE.

#### IV. CONCLUSIONS AND OUTLOOK

A combined experimental and theoretical approach has been used to investigate the performance of solvent models in describing the variations observed experimentally in the linear and nonlinear optical properties of push-pull probes (di-8-ANEPPS and DR1) in solution. The change in the (N)LO responses observed when moving from the isolated gas phase to solutions, as well as the statistical analysis, confirmed the importance of including the dynamical solvation effects in the calculations. The experimental data obtained by hyper-Rayleigh scattering are compared with theoretical TDDFT/M06-2X/6-311+G\* results using different solvent schemes (namely PCM, SMD, EE+PCM, and PE). All results reproduce the known unconventional solvatochromism of the ANEPP dye. Indeed, the absorption spectrum is blue-shifted as the solvent polarity is increased from  $\text{DCCl}_3$ , to Eth-OD, DMF, and DMSO. Among the continuum models, SMD performs slightly better than PCM, and by considering explicit solvent molecules represented by point charges around the probe (EE+PCM), quantitative agreement with experimental data is almost achieved. The polarizable embedding is also suitable for predicting LO properties. Concerning the evaluation of  $\beta_{\text{HRS}}$ , for both di-8-ANEPPS and DR1, PE gives the best individual results compared to experiment, and greatly reproduces the variations of the NLO responses when either the polarity of the solvent or the incident wavelength is switched. Still, EE+PCM already performs well.

In this work,  $\beta_{\text{HRS}}$  values were measured only in  $\text{DCCl}_3$ , DMF, and DMSO. These solvents are able to solubilize the ANEPP probe and have a transparent optical window to perform the measurements. Therefore, only aprotic solvents were investigated. In the future, protic solvents could also be considered, along with expanding the collection of aprotic solvents to further test the performance of the solvation schemes to reproduce the (N)LO responses of other dyes. Nevertheless, we have shown that the "intermediate" EE+PCM approach is an efficient choice for calculating (N)LO properties in solutions, and that PE works best.

#### ASSOCIATED CONTENT

Details about (i) the calculations parameters (reparameterization of GAFF for DR1 (Section S1.1) and PE parameters for DMF (Section S1.2)). (ii) the analysis of key relevant geometrical parameters (bond length alternation and torsion angles) (Tables S4 and S5 and Figures S3 and S4).

(ii) the linear optical responses in eV and nm (Table S6), the correlation between the absorption blue shifts and the solvent polarity indicator (Table S7 and Figure S5), the normalized experimental UV/Vis absorption spectra and their simulation using the different solvent models (Figure S6), the distribution of the lowest-energy allowed excitation energies and oscillator strengths (Figures S7-S11). (iv) the ground and excited states dipole moments (Table S8). (v) the charge transferred between the ground and excited states (Table S9). (vi) the total electronic energies (Figure S12). (vii) the HOMO-LUMO gaps (Figure S13). (viii) the experimental fluorescence (Figure S14 and Table S10) and IR spectra (Figure S15). (ix) the nonlinear optical responses: details about the HRS method, the calibration of the external reference DR1 (Figures S16-S19), the extrapolation of the external reference dispersion (Figure S20 and Table S12), the HRS results for di-8-ANEPPS (Table S13), the HRS power and polarization scans (Figures S21-S25), the correlation between measured and calculated  $\beta_{\text{HRS}}$  results (Tables S14, S15 and S16 and Figures S26 and S27), the  $\beta_{\text{HRS}}$  obtained via the TSA (Tables ??-?? and Figures ?? and ??), the  $\beta_{\text{HRS}}$  cumulative averages (Figures S28-S36), and the distribution of  $\beta_{\text{HRS}}$  (Figures S37-S45) and DR (Figures S46-S54).

## REFERENCES

- <sup>1</sup>M. G. Papadopoulos, A. J. Sadlej, and J. Leszczynski, eds., *Non-Linear Optical Properties of Matter. From Molecules to Condensed Phases* (Springer, 2006).
- <sup>2</sup>P. J. Campagnola, M.-d. Wei, A. Lewis, and L. M. Loew, *Biophys. J.* **77**, 3341 (1999).
- <sup>3</sup>J. E. Reeve, H. L. Anderson, and K. Clays, *Phys. Chem. Chem. Phys.* **12**, 13484 (2010).
- <sup>4</sup>M. Danko, P. Hrdlovič, A. Martinická, A. Benda, and M. Cigáň, *Photochem. Photobiol. Sci.* **16**, 1832 (2017).
- <sup>5</sup>M. Rajeshirke and N. Sekar, *Dye. Pigment.* **163**, 675 (2019).
- <sup>6</sup>L. H. Zucolotto Cocca, L. M. G. Abegão, L. F. Sciuti, R. Vabre, J. de Paula Siqueira, K. Kamada, C. R. Mendonca, S. Piguel, and L. De Boni, *J. Phys. Chem. C* **124**, 12617 (2020).
- <sup>7</sup>T. Pan, D. Lu, H. Xin, and B. Li, *Light Sci. Appl.* **10**, 124 (2021).
- <sup>8</sup>S. R. Marder, C. B. Gorman, F. Meyers, J. W. Perry, G. Bourhill, J.-L. Brédas, and B. M. Pierce, *Science* **265**, 632 (1994).
- <sup>9</sup>F. Meyers, S. R. Marder, B. M. Pierce, and J. L. Brédas, *J. Am. Chem. Soc.* **116**, 10703 (1994).
- <sup>10</sup>M. Ahlheim, M. Barzoukas, P. V. Bedworth, M. Blanchard-Desce, A. Fort, Z.-Y. Hu, S. R. Marder, J. W. Perry, C. Runser, M. Staehelin, and B. Zysset, *Science* **271**, 335 (1996).
- <sup>11</sup>W. H. Thompson, M. Blanchard-Desce, and J. T. Hynes, *J. Phys. Chem. A* **102**, 7712 (1998).
- <sup>12</sup>L. Dalton, A. Harper, A. Ren, F. Wang, G. Todorova, J. Chen, C. Zhang, and M. Lee, *Ind. Eng. Chem. Res.* **38**, 8 (1999).
- <sup>13</sup>M. Blanchard-Desce, J.-B. Baudin, L. Jullien, R. Lorne, O. Ruel, S. Brasselet, and J. Zyss, *Opt. Mater.* **12**, 333 (1999).
- <sup>14</sup>N. A. Murugan, J. Kongsted, Z. Rinkevicius, and H. Ågren, *Proc. Natl. Acad. Sci.* **107**, 16453 (2010).
- <sup>15</sup>F. Castet, M. Blanchard-Desce, F. Adamietz, Y. M. Poronik, D. T. Gryko, and V. Rodriguez, *Chem. Phys. Chem.* **15**, 2575 (2014).
- <sup>16</sup>F. Castet, A. Gillet, F. Bureš, A. Plaquet, V. Rodriguez, and B. Champagne, *Dyes and Pigments* **184**, 108850 (2021).
- <sup>17</sup>Y. Siqueira, M. L. Lyra, T. N. Ramos, B. Champagne, and V. Manzoni, *J. Chem. Phys.* **156**, 014305 (2022).
- <sup>18</sup>K. Clays and A. Persoons, *Phys. Rev. Lett.* **66**, 2980 (1991).

Sample title

- <sup>19</sup>C. Dehu, F. Meyers, E. Hendrickx, K. Clays, A. Persoons, S. R. Marder, and J. L. Brédas, J. Am. Chem. Soc. **117**, 10127 (1995).
- <sup>20</sup>P. Kaatz and D. P. Shelton, J. Chem. Phys. **105**, 3918 (1996).
- <sup>21</sup>F. L. Huyskens, P. L. Huyskens, and A. P. Persoons, J. Chem. Phys. **108**, 8161 (1998).
- <sup>22</sup>K. Clays, E. Hendrickx, M. Triest, T. Verbiest, A. Persoons, C. Dehu, and J.-L. Brédas, Science **262**, 1419 (1993).
- <sup>23</sup>G. Bourhill, J.-L. Brédas, L.-T. Cheng, S. R. Marder, F. Meyers, J. W. Perry, and B. G. Tiemann, J. Am. Chem. Soc. **116**, 2619 (1994).
- <sup>24</sup>M. A. Pauley, C. H. Wang, and A. K. Jen, J. Chem. Phys. **102**, 6400 (1995).
- <sup>25</sup>P. K. Das, J. Phys. Chem. B **110**, 7621 (2006).
- <sup>26</sup>V. Poltev, in *Handbook of Computational Chemistry*, edited by J. Leszczynski (Springer, 2012) pp. 259–292.
- <sup>27</sup>D. R. Kanis, M. A. Ratner, and T. J. Marks, Chem. Rev. **94**, 195 (1994).
- <sup>28</sup>A. Warshel and M. Levitt, J. Mol. Biol. **103**, 227 (1976).
- <sup>29</sup>H. Hodak, J. Mol. Biol. **426**, 1 (2014).
- <sup>30</sup>G. C. K. Roberts, ed., *Encyclopedia of Biophysics* (Springer Heidelberg, 2013).
- <sup>31</sup>J. M. Olsen, K. Aidas, and J. Kongsted, J. Chem. Theory Comput. **6**, 3721 (2010).
- <sup>32</sup>J. Tomasi, B. Mennucci, and R. Cammi, Chem. Rev. **105**, 2999 (2005).
- <sup>33</sup>S. Miertuš, E. Scrocco, and J. Tomasi, Chem. Phys. **55**, 117 (1981).
- <sup>34</sup>E. Cancès, B. Mennucci, and J. Tomasi, J. Chem. Phys. **107**, 3032 (1997).
- <sup>35</sup>B. Mennucci, Wiley Interdiscip. Rev. Comput. Mol. Sci. **2**, 386 (2012).
- <sup>36</sup>A. V. Marenich, C. J. Cramer, and D. G. Truhlar, J. Phys. Chem. B **113**, 6378 (2009).
- <sup>37</sup>J. Andzelm, C. Kölmel, and A. Klamt, J. Chem. Phys. **103**, 9312 (1995).
- <sup>38</sup>A. Klamt and V. Jonas, J. Chem. Phys. **105**, 9972 (1996).
- <sup>39</sup>A. Klamt, Wiley Interdiscip. Rev. Comput. Mol. Sci. **8**, 1 (2018).
- <sup>40</sup>J. R. Pliego and J. M. Riveros, Wiley Interdiscip. Rev. Comput. Mol. Sci. **10**, e1440 (2020).
- <sup>41</sup>G. Norjmaa, G. Ujaque, and A. Lledós, Top. Catal. **65**, 118 (2022).
- <sup>42</sup>L. W. Chung, W. M. Sameera, R. Ramozzi, A. J. Page, M. Hatanaka, G. P. Petrova, T. V. Harris, X. Li, Z. Ke, F. Liu, H. B. Li, L. Ding, and K. Morokuma, Chem. Rev. **115**, 5678 (2015).
- <sup>43</sup>K. V. Mikkelsen, Y. Luo, H. Ågren, and P. Jørgensen, J. Chem. Phys. **100**, 8240 (1994).
- <sup>44</sup>L. A. Junior, G. Colherinhas, T. L. Fonseca, and M. A. Castro, Chem. Phys. Lett. **598**, 43 (2014).

Sample title

- <sup>45</sup>J. Quertinmont, B. Champagne, F. Castet, and M. Hidalgo Cardenuto, *J. Phys. Chem. A* **119**, 5496 (2015).
- <sup>46</sup>S. Kothavale, S. Katariya, and N. Sekar, *Opt. Mater.* **75**, 379 (2018).
- <sup>47</sup>V. Manzoni, L. Modesto-Costa, J. Del Nero, T. Andrade-Filho, and R. Gester, *Opt. Mater.* **94**, 152 (2019).
- <sup>48</sup>C. Tonnelé, B. Champagne, L. Muccioli, and F. Castet, *Chem. Mater.* **31**, 6759 (2019).
- <sup>49</sup>G. Le Breton, O. Bonhomme, P. F. Brevet, E. Benichou, and C. Loison, *Phys. Chem. Chem. Phys.* **23**, 24932 (2021).
- <sup>50</sup>G. Le Breton, O. Bonhomme, E. Benichou, and C. Loison, *Phys. Chem. Chem. Phys.* **24**, 19463 (2022).
- <sup>51</sup>S. B. Allin, T. M. Leslie, and R. S. Lumpkin, *Chem. Mater.* **8**, 428 (1996).
- <sup>52</sup>J. Guthmuller and D. Simon, *J. Chem. Phys.* **124**, 174502 (2006).
- <sup>53</sup>D. H. Bale, B. E. Eichinger, W. Liang, X. Li, L. R. Dalton, B. H. Robinson, and P. J. Reid, *J. Phys. Chem. B* **115**, 3505 (2011).
- <sup>54</sup>F. Castet, E. Bogdan, A. Plaquet, L. Ducasse, B. Champagne, and V. Rodriguez, *J. Chem. Phys.* **136**, 024506 (2012).
- <sup>55</sup>T. Giovannini, M. Ambrosetti, and C. Cappelli, *Theor. Chem. Acc.* **137**, 1 (2018).
- <sup>56</sup>L. M. G. Abegão, R. D. Fonseca, F. A. Santos, J. J. Rodrigues, K. Kamada, C. R. Mendonça, S. Piguel, and L. De Boni, *RSC Adv.* **9**, 26476 (2019).
- <sup>57</sup>N. A. Murugan, R. Apostolov, Z. Rinkevicius, J. Kongsted, E. Lindahl, and H. Ågren, *J. Am. Chem. Soc.* **135**, 13590 (2013).
- <sup>58</sup>S. Osella and S. Knippenberg, *ACS Appl. Bio Mater.* **2**, 5769 (2019).
- <sup>59</sup>C. Bouquiaux, C. Tonnelé, F. Castet, and B. Champagne, *J. Phys. Chem. B* **124**, 2101 (2020).
- <sup>60</sup>C. Bouquiaux, F. Castet, and B. Champagne, *J. Phys. Chem. B* **125**, 10195 (2021).
- <sup>61</sup>C. Bouquiaux, F. Castet, and B. Champagne, *J. Phys. Chem. B* **127**, 528 (2023).
- <sup>62</sup>L. Ferrighi, L. Frediani, C. Cappelli, P. Sałek, H. Ågren, T. Helgaker, and K. Ruud, *Chem. Phys. Lett.* **425**, 267 (2006).
- <sup>63</sup>E. Benassi, F. Egidi, and V. Barone, *J. Phys. Chem. B* **119**, 3155 (2015).
- <sup>64</sup>M. F. Khan, R. B. Rashid, M. M. Rahman, M. A. Faruk, M. M. Rahman, and M. A. Rashid, *Int. J. Pharm. Pharm. Sci.* **9**, 217 (2017).
- <sup>65</sup>K. Pielak, C. Tonnelé, L. Sanguinet, E. Cariati, S. Righetto, L. Muccioli, F. Castet, and B. Champagne, *J. Phys. Chem. C* **122**, 26160 (2018).

Sample title

- <sup>66</sup>N. I. Shalin, Y. A. Phrolycheva, O. D. Fominykh, and M. Y. Balakina, *J. Mol. Liq.* **330**, 115665 (2021).
- <sup>67</sup>T. Ramos and B. Champagne, *ChemistryOpen* **12**, 15057 (e202200045).
- <sup>68</sup>R. Cammi, *Int. J. Quantum Chem.* **112**, 2547 (2012).
- <sup>69</sup>M. Barzoukas, C. Runser, A. Fort, and M. Blanchard-Desce, *Chem. Phys. Lett.* **257**, 531 (1996).
- <sup>70</sup>R. S. Ries, H. Choi, R. Blunck, F. Bezanilla, and J. R. Heath, *J. Phys. Chem. B* **108**, 16040 (2004).
- <sup>71</sup>J. E. Reeve, A. D. Corbett, I. Boczarow, T. Wilson, H. Bayley, and H. L. Anderson, *Biophys. J.* **103**, 907 (2012).
- <sup>72</sup>A. Khadria, Y. de Coene, P. Gawel, C. Roche, K. Clays, and H. L. Anderson, *Org. Biomol. Chem.* **15**, 947 (2017).
- <sup>73</sup>S.-N. Wu, M.-W. Lin, and Y.-J. Wang, *Pflügers Arch. - Eur. J. Physiol.* **455**, 687 (2007).
- <sup>74</sup>Q. Tian, M. Oberhofer, S. Ruppenthal, A. Scholz, V. Buschmann, H. Tsutsui, A. Miyawaki, A. Zeug, P. Lipp, and L. Kaestner, *Cell. Physiol. Biochem.* **27**, 281 (2011).
- <sup>75</sup>C. Manno, L. Figueroa, R. Fitts, and E. Ríos, *J. Gen. Physiol.* **141**, 371 (2013).
- <sup>76</sup>R. Cammi, B. Mennucci, J. Tomasi, V. Scienze, and C. Industriale, **7863**, 8834 (1998).
- <sup>77</sup>P. Hrobárik, I. Sigmundová, P. Zahradník, P. Kasák, V. Arion, E. Franz, and K. Clays, *J. Phys. Chem. C* **114**, 22289 (2010).
- <sup>78</sup>B. Jędrzejewska, P. Krawczyk, M. Pietrzak, M. Gordel, K. Matczyszyn, M. Samoć, and P. Cysewski, *Dyes Pigm.* **99**, 673 (2013).
- <sup>79</sup>P. K. Samanta, M. M. Alam, R. Misra, and S. K. Pati, *Phys. Chem. Chem. Phys.* **21**, 17343 (2019).
- <sup>80</sup>M. Zhang, M. Wang, Y. Guo, Y. Shi, J. Wang, Y. Chen, C. Zhao, Y. Zhou, Y. Xiao, H. Zhang, and G. Zhao, *Spectrochim. Acta Part A Mol. Biomol. Spectrosc.* **260**, 119949 (2021).
- <sup>81</sup>X. Cao, R. W. Tolbert, J. L. McHale, and W. D. Edwards, *J. Phys. Chem. A* **102**, 2739 (1998).
- <sup>82</sup>L. Wang, Q. Chen, G. Zhai, Z. Wen, and Z. Zhang, *J. Mol. Struct. THEOCHEM* **778**, 15 (2006).
- <sup>83</sup>P. S. Kumar, K. Vasudevan, A. Prakasam, M. Geetha, and P. Anbarasan, *Spectrochim. Acta Part A Mol. Biomol. Spectrosc.* **77**, 45 (2010).
- <sup>84</sup>S. Stadler, R. Dietrich, G. Bourhill, and C. Bräuchle, *Opt. Lett.* **21**, 251 (1996).
- <sup>85</sup>M. A. Pauley and C. H. Wang, *Chem. Phys. Lett.* **280**, 544 (1997).

Sample title

- <sup>86</sup>M. A. Pauley and C. H. Wang, *Rev. Sci. Instrum.* **70**, 1277 (1999).
- <sup>87</sup>C. Wang, J. Woodford, and A. K.-Y. Jen, *Chem. Phys.* **262**, 475 (2000).
- <sup>88</sup>C.-C. Hsu, S. Liu, C. C. Wang, and C. H. Wang, *J. Chem. Phys.* **114**, 7103 (2001).
- <sup>89</sup>C. H. Wang, Y. C. Lin, O. Y. Tai, and A. K.-Y. Jen, *J. Chem. Phys.* **119**, 6237 (2003).
- <sup>90</sup>O. Y.-H. Tai, C. H. Wang, H. Ma, and A. K.-Y. Jen, *J. Chem. Phys.* **121**, 6086 (2004).
- <sup>91</sup>S. K. Yang, H. C. Ahn, S.-j. Jeon, I. Asselberghs, K. Clays, A. Persoons, and B. R. Cho, *Chem. Phys. Lett.* **403**, 68 (2005).
- <sup>92</sup>H. Li, G. Mao, K. D. Singer, Z. Lu, R. Weber, and R. J. Twieg, *J. Opt. Soc. Am. B* **24**, 1310 (2007).
- <sup>93</sup>J. Campo, F. Desmet, W. Wenseleers, and E. Goovaerts, *Opt. Express* **17**, 4587 (2009).
- <sup>94</sup>T. Verbiest, K. Clays, and V. Rodriguez, *Second-Order Nonlinear Optical Characterization Techniques: an Introduction* (CRC Press, 2009).
- <sup>95</sup>M. Büchert, T. Steenbock, C. Lukaschek, M. C. Wolff, C. Herrmann, and J. Heck, *Chem. Eur. J.* **20**, 14351 (2014).
- <sup>96</sup>L.-t. Cheng, W. Tam, S. H. Stevenson, G. R. Meredith, and S. R. Marder, *J. Phys. Chem.* **95**, 10631 (1991).
- <sup>97</sup>S. Stadler, F. Feiner, C. Br, S. Brandl, and R. Gompper, *Chem. Phys. Lett.* **245**, 292 (1995).
- <sup>98</sup>S. F. Hubbard, R. G. Petschek, and K. D. Singer, *Opt. Lett.* **21**, 1774 (1996).
- <sup>99</sup>S. Wong and K. Wong, *Opt. Commun.* **133**, 268 (1997).
- <sup>100</sup>C. H. Wang, J. N. Woodford, C. Zhang, and L. R. Dalton, *J. Appl. Phys.* **89**, 4209 (2001).
- <sup>101</sup>J. Brunel, A. Jutand, I. Ledoux, J. Zyss, and M. Blanchard-Desce, *Synth. Met.* **124**, 195 (2001).
- <sup>102</sup>Y. Liao, K. A. Firestone, S. Bhattacharjee, J. Luo, M. Haller, S. Hau, C. A. Anderson, D. Lao, B. E. Eichinger, B. H. Robinson, P. J. Reid, A. K.-Y. Jen, and L. R. Dalton, *J. Phys. Chem. B* **110**, 5434 (2006).
- <sup>103</sup>M. He, Y. Zhou, R. Liu, J. Dai, Y. Cui, and T. Zhang, *Dyes and Pigments* **80**, 6 (2009).
- <sup>104</sup>F. Castet, C. Tonnelé, L. Muccioli, and B. Champagne, *Acc. Chem. Res.* **55**, 3716 (2022).
- <sup>105</sup>R. W. Terhune, P. D. Maker, and C. M. Savage, *Phys. Rev. Lett.* **14**, 681 (1965).
- <sup>106</sup>R. Bersohn, Y. Pao, and H. L. Frisch, *J. Chem. Phys.* **45**, 3184 (1966).
- <sup>107</sup>G. J. T. Heesink, A. G. T. Ruiter, N. F. van Hulst, and B. Bölger, *Phys. Rev. Lett.* **71**, 999 (1993).
- <sup>108</sup>I. D. Morrison, R. G. Denning, W. M. Laidlaw, and M. A. Stammers, *Rev. Sci. Instrum.* **67**, 1445 (1996).

Sample title

- <sup>109</sup>J. Quertinmont, P. Beaujean, J. Stiennon, Y. Aidibi, P. Leriche, V. Rodriguez, L. Sanguinet, and B. Champagne, *J. Phys. Chem. B* **125**, 3918 (2021).
- <sup>110</sup>S. Dubuis, A. Dellai, C. Courdurié, J. Owona, A. Kalafatis, L. Vellutini, E. Genin, V. Rodriguez, and F. Castet, *J. Am. Chem. So.* **145**, 10861 (2023).
- <sup>111</sup>M. A. Pauley, H. Guan, C. H. Wang, and A. K. Jen, *J. Chem. Phys.* **104**, 7821 (1996).
- <sup>112</sup>E. Hendrickx, K. Clays, and A. Persoons, *Acc. Chem. Res.* **31**, 675 (1998).
- <sup>113</sup>J. C. Phillips, R. Braun, W. Wang, J. Gumbart, E. Tajkhorshid, E. Villa, C. Chipot, R. D. Skeel, L. Kalé, and K. Schulten, *J. Comput. Chem.* **26**, 1781 (2005).
- <sup>114</sup>W. Humphrey, A. Dalke, and K. Schulten, *J. Molec. Graphics* **14**, 33 (1996).
- <sup>115</sup>L. Martínez, R. Andrade, E. G. Birgin, and J. M. Martínez, *J. Comput. Chem.* **30**, 2157 (2009).
- <sup>116</sup>D. R. Lide, ed., *CRC Handbook of Chemistry and Physics*, 76th ed. (CRC Press, 2005).
- <sup>117</sup>S. E. Feller, Y. Zhang, R. W. Pastor, and B. R. Brooks, *J. Chem. Phys.* **103**, 4613 (1995).
- <sup>118</sup>S. Piana, K. Lindorff-Larsen, R. M. Dirks, J. K. Salmon, R. O. Dror, and D. E. Shaw, *PLoS One* **7**, 1 (2012).
- <sup>119</sup>U. Essmann, L. Perera, and M. L. Berkowitz, *J. Chem. Phys.* **103**, 8577 (1995).
- <sup>120</sup>S. J. Weiner, P. A. Kollman, U. C. Singh, D. A. Case, C. Ghio, G. Alagona, S. Profeta, and P. Weiner, *J. Am. Chem. Soc.* **106**, 765 (1984).
- <sup>121</sup>J. Wang, R. M. Wolf, J. W. Caldwell, P. A. Kollman, and D. A. Case, *J. Comput. Chem.* **25**, 1157 (2004).
- <sup>122</sup>C. Desfrancois, V. Périquet, S. Carles, J. P. Schermann, and L. Adamowicz, *Chem. Phys.* **239**, 475 (1998).
- <sup>123</sup>J. Comer, J. C. Gumbart, J. Hénin, T. Lelièvre, A. Pohorille, and C. Chipot, *J. Phys. Chem. B* **119**, 1129 (2014).
- <sup>124</sup>M. J. Frisch, G. W. Trucks, H. B. Schlegel, G. E. Scuseria, M. A. Robb, J. R. Cheeseman, G. Scalmani, V. Barone, G. A. Petersson, H. Nakatsuji, X. Li, M. Caricato, A. V. Marenich, J. Bloino, B. G. Janesko, R. Gomperts, B. Mennucci, H. P. Hratchian, J. V. Ortiz, A. F. Izmaylov, J. L. Sonnenberg, D. Williams-Young, F. Ding, F. Lipparini, F. Egidi, J. Goings, B. Peng, A. Petrone, T. Henderson, D. Ranasinghe, V. G. Zakrzewski, J. Gao, N. Rega, G. Zheng, W. Liang, M. Hada, M. Ehara, K. Toyota, and R. Fukuda, “Gaussian 16 Revision A.03,” (2016), gaussian Inc. Wallingford CT.
- <sup>125</sup>L. E. Johnson, L. R. Dalton, and B. H. Robinson, *Acc. Chem. Res.* **47**, 3258 (2014).
- <sup>126</sup>R. S. Roy and P. K. Nandi, *RSC Adv.* **5**, 103729 (2015).

Sample title

- <sup>127</sup>L. M. G. Abegão, R. D. Fonseca, F. A. Santos, J. J. Rodrigues, K. Kamada, C. R. Mendonça, S. Piguel, and L. De Boni, *RSC Adv.* **9**, 26476 (2019).
- <sup>128</sup>N. I. Shalin, O. D. Fominykh, and M. Y. Balakina, *Chem. Phys. Lett.* **717**, 21 (2019).
- <sup>129</sup>L. Lescos, S. P. Sitkiewicz, P. Beaujean, M. Blanchard-Desce, B. Champagne, E. Matito, and F. Castet, *Phys. Chem. Chem. Phys.* **22**, 16579 (2020).
- <sup>130</sup>T. Hrivnák, M. Medved', W. Bartkowiak, and R. Zaleśny, *Molecules* **27**, 8738 (2022).
- <sup>131</sup>I. Brandão, T. L. Fonseca, L. R. Franco, H. C. Georg, and M. A. Castro, *Chem. Phys. Lett.* **796**, 139549 (2022).
- <sup>132</sup>M. de Wergifosse and B. Champagne, *J. Chem. Phys.* **134**, 074113 (2011).
- <sup>133</sup>A. Karakaş, Z. E. Koç, M. Fridrichová, P. Němetec, and J. Kroupa, *J. Theor. Comput. Chem.* **11**, 209 (2012).
- <sup>134</sup>B. Mennucci, E. Cancès, and J. Tomasi, *J. Chem. Phys. B* **101**, 10506 (1997).
- <sup>135</sup>J. Tomasi, B. Mennucci, and R. Cammi, *Chem. Rev.* **105**, 2999 (2005).
- <sup>136</sup>S. Miertus, E. Scrocco, and J. Tomasi, *Chem. Phys.* **55**, 117 (1981).
- <sup>137</sup>M. F. Khan, R. B. Rashid, M. A. Hossain, and M. A. Rashid, *Dhaka Univ. J. Pharm. Sci.* **16**, 1 (2017).
- <sup>138</sup>L. Ahmed and R. Omer, *J. Phys. Chem. Funct. Mater.* **4**, 10 (2021).
- <sup>139</sup>X. Q. Li, C. H. Wang, M. Y. Zhang, H. Y. Zou, N. N. Ma, and Y. Q. Qiu, *J. Organomet. Chem.* **749**, 327 (2014).
- <sup>140</sup>M. J. Kariyottu Kuniyil and R. Padmanaban, *New J. Chem.* **43**, 13616 (2019).
- <sup>141</sup>A. H. AlSilaykhee, A. Al-Yasari, and H. F. Alesary, *Int. J. Quantum Chem.* **123**, e27086 (2023).
- <sup>142</sup>J. M. H. Olsen and J. Kongsted, in *Advances in Quantum Chemistry*, Vol. 61, edited by J. R. Sabin and E. Brändas (Elsevier Inc., 2011) pp. 107–143.
- <sup>143</sup>K. Aidas, C. Angeli, K. L. Bak, V. Bakken, R. Bast, L. Boman, O. Christiansen, R. Cimiraglia, E. K. Dalskov, U. Ekstr, S. Coriani, T. Enevoldsen, J. J. Eriksen, P. Ettenhuber, B. Fern, L. Ferrighi, H. Fliegl, L. Frediani, E. Hjertenæs, S. Høst, I.-m. Høyvik, D. Jonsson, P. Jørgensen, J. Kauczor, S. Kirpekar, T. Kjærgaard, W. Klopper, S. Knecht, R. Kobayashi, H. Koch, J. Kongsted, A. Krapp, K. Kristensen, A. Ligabue, O. B. Lutnæs, J. I. Melo, K. V. Mikkelsen, R. H. Myhre, C. Neiss, C. B. Nielsen, P. Norman, M. H. Olsen, A. Osted, P. F. Provasi, S. Reine, Z. Rinkevicius, K. Snegov, A. H. Steindal, K. O. Sylvester-hvid, P. R. Taylor, A. M. Teale, E. I. Tellgren, D. P. Tew, A. J. Thorvaldsen, L. Thøgersen, O. Vahtras, M. A. Watson, and D. J. D. Wilson, *Wiley Interdiscip. Rev. Comput. Mol. Sci.* **4**, 269 (2014).

Sample title

- <sup>144</sup>C. I. Bayly, P. Cieplak, W. Cornell, and P. A. Kollman, *J. Phys. Chem.* **97**, 10269 (1993).
- <sup>145</sup>M. T. P. Beerepoot, A. H. Steindal, N. H. List, J. Kongsted, and J. M. H. Olsen, *J. Chem. Theory Comput.* **12**, 1684 (2016).
- <sup>146</sup>J. L. Oudar and D. S. Chemla, *J. Chem. Phys.* **66**, 2664 (1977).
- <sup>147</sup>X. Cao and J. L. McHale, *J. Chem. Phys.* **109**, 1901 (1998).
- <sup>148</sup>H. Li, G. Mao, and K. D. Singer, in *Optical Molecular Probes for Biomedical Applications*, Vol. 6097, edited by S. Achilefu, D. J. Bornhop, and R. Raghavachari (2006) p. 609705.
- <sup>149</sup>M. Panigrahi, S. Patel, and B. K. Mishra, *J. Mol. Liq.* **177**, 335 (2013).
- <sup>150</sup>S. Yordanova, I. Petkov, and S. Stoyanov, *J. Chem. Technol. Metall.* **49**, 601 (2014).
- <sup>151</sup>C. Reichardt, *Chem. Rev.* **94**, 2319 (1994).
- <sup>152</sup>P. Fromherz, *J. Phys. Chem.* **99**, 7188 (1995).
- <sup>153</sup>L. M. Loew, L. Simpson, A. Hassner, and V. Alexanian, *J. Am. Chem. Soc.* **101**, 5439 (1979).
- <sup>154</sup>E. Fluhler, V. G. Burnham, and L. M. Loew, *Biochemistry* **24**, 5749 (1985).
- <sup>155</sup>H. Ephardt and P. Fromherz, *J. Phys. Chem.* **95**, 6792 (1991).
- <sup>156</sup>P. Hébert, G. Baldacchino, T. Gustavsson, and J. Mialocq, *J. Photochem. Photobiol. A Chem.* **84**, 45 (1994).
- <sup>157</sup>D. Laage, W. H. Thompson, M. Blanchard-Desce, and J. T. Hynes, *J. Phys. Chem. A* **107**, 6032 (2003).
- <sup>158</sup>N. S. Bayliss and E. G. McRae, *J. Phys. Chem.* **58**, 1002 (1954).
- <sup>159</sup>S. Bai, R. Mansour, L. Stojanović, J. M. Toldo, and M. Barbatti, *J. Mol. Model.* **26**, 107 (2020).
- <sup>160</sup>B. Lasorne, J. Jorner-Somoza, H.-D. Meyer, D. Lauvergnat, M. A. Robb, and F. Gatti, *Spectrochim. Acta Part A Mol. Biomol. Spectrosc.* **119**, 52 (2014).
- <sup>161</sup>B. Champagne, M. Guillaume, and F. Zutterman, *Chem. Phys. Lett.* **425**, 105 (2006).
- <sup>162</sup>M. Guillaume, B. Champagne, and F. Zutterman, *J. Phys. Chem. A* **110**, 13007 (2006).
- <sup>163</sup>B. Champagne, V. Liégeois, and F. Zutterman, *Photochem. Photobiol. Sci.* **14**, 444 (2015).
- <sup>164</sup>F. Zutterman, V. Liégeois, and B. Champagne, *ChemPhotoChem* **1**, 281 (2017).
- <sup>165</sup>T. Kodaira, A. Watanabe, O. Ito, M. Matsuda, K. Clays, and A. Persoons, *J. Chem. Soc. Faraday Trans.* **93**, 3039 (1997).
- <sup>166</sup>O. K. Song, J. N. Woodford, and C. H. Wang, *J. Phys. Chem. A* **101**, 3222 (1997).
- <sup>167</sup>T. W. Chui and K. Y. Wong, *J. Chem. Phys.* **109**, 1391 (1998).
- <sup>168</sup>C.-z. Zhang, C. Lu, J. Zhu, G.-y. Lu, X. Wang, Z.-w. Shi, F. Liu, and Y. Cui, *Chem. Mater.* **18**, 6091 (2006).

Sample title

- <sup>169</sup>S. J. Lalama and A. F. Garito, *Phys. Rev. A* **20**, 1179 (1979).
- <sup>170</sup>S. P. Karna, P. N. Prasad, and M. Dupuis, *J. Chem. Phys.* **94**, 1171 (1991).
- <sup>171</sup>J. L. Brédas, F. Meyers, B. M. Pierce, and J. Zyss, *J. Am. Chem. Soc.* **114**, 4928 (1992).
- <sup>172</sup>F. Sim, S. Chin, M. Dupuis, and J. E. Rice, *J. Phys. Chem.* **97**, 1158 (1993).
- <sup>173</sup>M. Zakerhamidi, M. Keshavarz, H. Tajalli, A. Ghanadzadeh, S. Ahmadi, M. Moghadam, S. Hosseini, and V. Hooshangi, *J. Mol. Liq.* **154**, 94 (2010).
- <sup>174</sup>M. Makowska-Janusik and J.-F. Benard, *J. Phys. Conf. Ser.* **79**, 012030 (2007).
- <sup>175</sup>J. Carmona-Espíndola, R. Flores-Moreno, and A. M. Köster, *Int. J. Quantum Chem.* **112**, 3461 (2012).
- <sup>176</sup>E. Marcano, E. Squitieri, J. Murgich, and H. Soscún, *Comput. Theor. Chem.* **985**, 72 (2012).
- <sup>177</sup>B. Raaghul, M. Kannan, and T. Vijayakumar, *IOP Conf. Ser. Mater. Sci. Eng.* **1219**, 012035 (2022).
- <sup>178</sup>Y. Zhao and D. G. Truhlar, *Theor. Chem. Account* , 215 (2008).
- <sup>179</sup>Y. Zhao, N. E. Schultz, and D. G. Truhlar, *J. Chem. Theory Comput.* , 364 (2006).
- <sup>180</sup>A. J. Cohen, P. Mori-Sánchez, and W. Yang, *Chem. Rev.* , 289 (2012).
- <sup>181</sup>K. Clays, A. Persoons, and L. D. Maeyer, *Advances in Chemical Physics*, Vol. 85 (Wiley, New-York, 1994) pp. 455–498.
- <sup>182</sup>L. M. Loew, *Pure Appl. Chem.* **68**, 1405 (1996).
- <sup>183</sup>J. A. Giordmaine, *Phys. Rev.* **138**, A1599 (1965).
- <sup>184</sup>F. Helmchen and W. Denk, *Nat. Methods* **2**, 932 (2005).
- <sup>185</sup>F. Ding, J. Feng, X. Zhang, J. Sun, C. Fan, and Z. Ge, *Adv. Drug Deliv. Rev.* **173**, 141 (2021).
- <sup>186</sup>A. K. Barik, M. Sanoop Pavithran, J. Lukose, R. Upadhyaya, M. V. Pai, V. B. Kartha, and S. Chidangil, *Expert Rev. Med. Devices* **19**, 657 (2022).
- <sup>187</sup>S. X. Han, X. Jia, J. L. Ma, and Q. Zhu, *Arch. Immunol. Ther. Exp. (Warsz)*. **61**, 139 (2013).
- <sup>188</sup>Z. Kejík, R. Kaplánek, M. Havlík, T. Bříza, M. Jakubek, J. Králová, I. Mikula, P. Martásek, and V. Král, *Bioorganic Med. Chem.* **25**, 2295 (2017).
- <sup>189</sup>S. B. Raymond, J. Skoch, I. D. Hills, E. E. Nesterov, T. M. Swager, and B. J. Bacskai, *Eur. J. Nucl. Med. Mol. Imaging* **35**, 93 (2008).
- <sup>190</sup>X. Zhen and X. Jiang, *Wiley Interdiscip. Rev. Nanomedicine Nanobiotechnology* **12**, 1 (2020).
- <sup>191</sup>C. Martelli, A. Lo Dico, C. Diceglie, G. Lucignani, and L. Ottobriani, *Oncotarget* **7**, 48753 (2016).

Sample title

- <sup>192</sup>J. Neugebauer, M. J. Louwarse, E. J. Baerends, T. A. Wesolowski, J. Neugebauer, M. J. Louwarse, and E. Jan, **094115** (2014), 10.1063/1.1858411.
- <sup>193</sup>R. H. C. Janssen, J. Bomont, D. N. Theodorou, S. Raptis, and M. G. Papadopoulos, **6463** (2014), 10.1063/1.478549.
- <sup>194</sup>C. Steinmann, P. Reinholdt, M. S. Nørby, J. Kongsted, and J. M. H. Olsen, *Int. J. Quantum Chem.* **119**, 1 (2019), arXiv:1804.03598.
- <sup>195</sup>C. J. Cramer and D. G. Truhlar, *Chem. Rev.* **99**, 2161 (1999).
- <sup>196</sup>H. P. Li, Z. T. Bi, W. Y. Fu, R. F. Xu, Y. Zhang, X. P. Shen, M. X. Li, G. Tang, and K. Han, *J. Mol. Model.* **23** (2017), 10.1007/s00894-017-3267-2.
- <sup>197</sup>S. Petralia and G. Forte, *J. Phys. Org. Chem.* **36**, e4443 (2023).
- <sup>198</sup>Y. Yang, Z. Guangrong, W. Xiaojing, and W. Gu, *J. Biomol. Struct. Dyn.* **40**, 7274 (2022).
- <sup>199</sup>A. Mubarik, N. Rasool, M. A. Hashmi, A. Mansha, M. Zubair, M. R. Shaik, M. A. Sharaf, E. M. Awwad, and A. Abdelgawad, *Crystals* **11**, 1 (2021).
- <sup>200</sup>R. Srivastava, F. A. Al-Omary, A. A. El-Emam, S. K. Pathak, M. Karabacak, V. Narayan, S. Chand, O. Prasad, and L. Sinha, *J. Mol. Struct.* **1137**, 725 (2017).
- <sup>201</sup>M. Lequan, C. Branger, J. Simon, T. Thami, E. Chauchard, and A. Persoons, *Chem. Phys. Lett.* **229**, 101 (1994).
- <sup>202</sup>P. Boldt, G. Bourhill, C. Bräuchle, Y. Jim, R. Kammler, C. Müller, J. Rase, and J. Wichern, *Chem. Commun.*, 793 (1996).
- <sup>203</sup>M. Tsukada, Y. Mineo, and K. Itoh, *J. Phys. Chem.* **93**, 7989 (1989).
- <sup>204</sup>K. Shibasaki and K. Itoh, *J. Raman Spectrosc.* **22**, 753 (1991).
- <sup>205</sup>M. D. Lechner, ed., *Static Dielectric Constants of Pure Liquids and Binary Liquid Mixtures* (Springer-Verlag, Berlin, Heidelberg, 2008).
- <sup>206</sup>A. P. Gregory, R. N. Clarke, and M. G. Cox, *Meas. Sci. Technol.* **20**, 075106 (2009).
- <sup>207</sup>P. Atkins and J. de Paula, eds., *Atkins's Physical Chemistry*, 8th ed. (Oxford University Press, 2006).
- <sup>208</sup>J. Hunger, R. Buchner, M. E. Kandil, E. F. May, K. N. Marsh, and G. Hefter, *J. Chem. Eng. Data* **55**, 2055 (2010).
- <sup>209</sup>L. Gagliardi, R. Lindh, and G. Karlström, *J. Chem. Phys.* **121**, 4494 (2004).
- <sup>210</sup>U. C. Singh and P. A. Kollman, *J. Comput. Chem.* **5**, 129 (1984).
- <sup>211</sup>B. H. Besler, K. M. Merz, and P. A. Kollman, *J. Comput. Chem.* **11**, 431 (1990).
- <sup>212</sup>J. Wang, W. Wang, P. A. Kollman, and D. A. Case, *J. Mol. Graph. Model.* **25**, 247 (2006).

Sample title

- <sup>213</sup>D. Case, H. Aktulga, K. Belfon, I. Ben-Shalom, J. Berryman, S. Brozell, D. Cerutti, T. Cheatham, III, G. Cisneros, V. Cruzeiro, T. Darden, R. Duke, G. Giambasu, M. Gilson, H. Gohlke, A. Goetz, R. Harris, S. Izadi, S. Izmailov, K. Kasavajhala, M. Kaymak, E. King, A. Kovalenko, T. Kurtzman, T. Lee, S. LeGrand, P. Li, C. Lin, J. Liu, T. Luchko, R. Luo, M. Machado, V. Man, M. Manathunga, K. Merz, Y. Miao, O. Mikhailovskii, G. Monard, H. Nguyen, K. O’Hearn, A. Onufriev, F. Pan, S. Pantano, R. Qi, A. Rahnamoun, D. Roe, A. Roitberg, C. Sagui, S. Schott-Verdugo, A. Shajan, J. Shen, C. Simmerling, N. Skrynnikov, J. Smith, J. Swails, R. Walker, J. Wang, J. Wang, H. Wei, R. Wolf, X. Wu, Y. Xiong, Y. Xue, D. York, S. Zhao, , and P. Kollman, “Amber 2022,” (2022), university of California, San Francisco.
- <sup>214</sup>D. A. Case, T. E. Cheatham, T. Darden, H. Gohlke, R. Luo, K. M. Merz, A. Onufriev, C. Simmerling, B. Wang, and R. J. Woods, *J. Comput. Chem.* **26**, 1668 (2005), arXiv:NIHMS150003.
- <sup>215</sup>O. Vahtras, “Loprop for dalton,” (2014).
- <sup>216</sup>K. Binnemans, C. Bex, A. Venard, H. De Leebeeck, and C. Görrler-Walrand, *J. Mol. Liq.* **83**, 283 (1999).
- <sup>217</sup>F. Moyano, J. J. Silber, and N. M. Correa, *J. Colloid Interface Sci.* **317**, 332 (2008).
- <sup>218</sup>D. M. Bishop, *Int. Rev. Phys. Chem.* **13**, 21 (1994).
- <sup>219</sup>J. Campo, W. Wenseleers, E. Goovaerts, M. Szablewski, and G. H. Cross, *J. Phys. Chem. C* **112**, 287 (2008).
- <sup>220</sup>T. Yamada, I. Aoki, H. Miki, C. Yamada, and A. Otomo, *Mater. Chem. Phys.* **139**, 699 (2013).
- <sup>221</sup>A. C. Millard, M. Terasaki, and L. M. Loew, *Biophys. J.* **88**, L46 (2005).
- <sup>222</sup>A. Obaid, L. Loew, J. Wuskell, and B. Salzberg, *J. Neurosci. Methods* **134**, 179 (2004).
- <sup>223</sup>G. Pucihar, T. Kotnik, and D. Miklavčič, *J. Vis. Exp.* , 2009 (2009).
- <sup>224</sup>Y. Hayashi, M. Zviman, J. Brand, J. Teeter, and D. Restrepo, *Biophys. J.* **71**, 1057 (1996).
- <sup>225</sup>P. O’Shea, *Biochem. Soc. Trans.* **31**, 990 (2003).
- <sup>226</sup>E. D. McGahren, J. M. Beach, and B. R. Duling, *Am. J. Physiol. Circ. Physiol.* **274**, H60 (1998).
- <sup>227</sup>T. Nakagawa, J. S. Oghalai, P. Saggau, R. D. Rabbitt, and W. E. Brownell, *J. Neural Eng.* **3**, 79 (2006).
- <sup>228</sup>M. DiFranco, M. Quinonez, J. Capote, and J. Vergara, *J. Vis. Exp.* , 1 (2009).
- <sup>229</sup>S. Kim, H. Moon, J. Hwang, J. Sohn, J. Seo, S. Y. Park, T. Im Kang, and B. Rae Cho, *Chem. Phys.* **256**, 289 (2000).

Sample title

- <sup>230</sup>A. Abbotto, L. Beverina, R. Bozio, S. Bradamante, C. Ferrante, G. A. Pagani, and R. Signorini, *Adv. Mater.* **12**, 1963 (2000).
- <sup>231</sup>H. Song, K. Wang, Z. Kuang, Y. S. Zhao, Q. Guo, and A. Xia, *Phys. Chem. Chem. Phys.* **21**, 3894 (2019).
- <sup>232</sup>J.-c. Mialocq, S. Pommeret, R. Naskrecki, G. Baldacchino, and T. Gustavsson, in *5th Int. Conf. Laser Appl. Life Sci.*, Vol. 2370, edited by P. A. Apanasevich, N. I. Koroteev, S. G. Kruglik, and V. N. Zadkov (1995) pp. 253–262.
- <sup>233</sup>M. Muniz-Miranda, T. Del Rosso, E. Giorgetti, G. Margheri, G. Ghini, and S. Cicchi, *Anal. Bioanal. Chem.* **400**, 361 (2011).
- <sup>234</sup>V. Gopi, S. Subbiahraj, K. Chemmanghattu, and P. C. Ramamurthy, *Dye. Pigment.* **173**, 107887 (2020).
- <sup>235</sup>S. Achelle, C. Baudequin, and N. Plé, *Dye. Pigment.* **98**, 575 (2013).
- <sup>236</sup>G. Olbrechts, K. Wostyn, K. Clays, and A. Persoons, *Opt. Lett.* **24**, 403 (1999).
- <sup>237</sup>H. Reis, *J. Chem. Phys.* **125**, 014506 (2006).
- <sup>238</sup>V. Rodriguez, J. Grondin, F. Adamietz, and Y. Danten, *J. Phys. Chem. B* **114**, 15057 (2010).
- <sup>239</sup>O. Ciocirlan and O. Iulian, *J. Serbian Chem. Soc.* **74**, 317 (2009).